Mutant screen reveals depression-associated *Piccolo's* control over brain-gonad cross talk and reproductive behavior

Gerardo A. Medrano[1&], Manvendra Singh[11&], Erik J. Plautz[6], Levi B. Good[6], Karen M. Chapman[1], Jaideep Chaudhary[1], Priscilla Jaichander[1], Heather M. Powell[1], Ashutosh Pudasaini[2], John M. Shelton[3], James A. Richardson[4,5], Xian-Jin Xie[7], Zoltán Ivics[9], Christine Braun[10], Frauke Ackermann[10], Craig C. Garner[10], Zsuzsanna Izsvák[11,*] and F. Kent Hamra[1, 2, 8,*]

Departments of [1]Pharmacology, [2]Obstetrics & Gynecology, Internal Medicine - Division of [3]Cardiology, [4]Pathology, [5]Molecular Biology, Neurology and [6]Neurotherapeutics, [7]Simmons Comprehensive Cancer Center, [8]Cecil H & Ida Green Center for Reproductive Biology Sciences, University of Texas Southwestern Medical Center in Dallas, USA; [9]Paul-Ehrlich-Institute, Division of Medical Biotechnology, Langen, Germany, German Center for Neurodegenerative Diseases (DZNE), [10]Charité Medical University, Charitéplatz 1, 10117 Berlin, Germany, [11]Max Delbrück Center for Molecular Medicine in the Helmholtz Society, Berlin, Germany

[&]equal contribution

[*]Address Correspondence to:

F. Kent Hamra
Department Obstetrics and Gynecology
Cecil H & Ida Green Center for Reproductive Biology Sciences
UT Southwestern Medical Center
5323 Harry Hines Blvd.
Dallas, Texas 75390

Telephone: (214) 648-2309
Fax: (214) 648-9242
Email: kent.hamra@utsouthwestern.edu

Zsuzsanna Izsvák
Max Delbrück Center for Molecular Medicine
in the Helmholtz Society
Robert Rössle Str. 10
D-13092 Berlin, Germany

Telephone: (49) 30 9406-3510
FAX: (49) 30 9406-2547
Email: www.mdc-berlin.de/izsvak

Short Title: Rat Genetics Unveils *Pclo* Pleiotropy

Key Words: reproduction, social behavior, affective disorders, conspecific recognition, mating, aggression, depression, seizures, epilepsy, GABAergic, olfactory, limbic system, hypothalamus, amygdala, forward genetics, *Sleeping Beauty* transposon, gene-trap, mutagenesis, pleiotropy, autophagy, spermatogonial, spermatogenesis

Abstract

Successful sexual reproduction involves complex, genetically encoded interplay between animal physiology and behavior. Here, we report an unbiased forward genetics screen to identify genes that regulate rat reproduction based on mutagenesis via the *Sleeping Beauty* transposon. As expected, our screen identified genes where reproductive failure was connected to gametogenesis (*Btrc*, *Pan3*, *Spaca6*, *Ube2k*) and embryogenesis (*Alk3*, *Exoc6b*, *Slc1a3*, *Tmx4*, *Zmynd8*). In addition, we identified *Atg13* (longevity) and *Pclo* (neuronal disorders), previously not associated with an inability to conceive. Dominant *Pclo* traits caused epileptiform activity and affected genes supporting GABAergic synaptic transmission (*Gabra6, Gabrg3*). Recessive *Pclo* traits transmitted altered reproductive behavior, including reduced sexual motivation and increased aggression. *Pclo* mutant behavior was linked to hypothalamic markers for negative energy, compromised brain-gonad crosstalk via disturbed GnRH signaling and allelic markers for major depressive disorder (*Grm5*, *Htr2a, Sorcs3, Negr1, Drd2)*. Thus, *Pclo* is a chemosensory-neuroendocrine regulatory factor that calibrates behavioral responses for reproduction.

Introduction

While a failure to reproduce sexually is often connected to physiological or developmental problems of the gonad, gamete or embryo, it is also commonly accepted that problems with sexual reproduction can be linked to various behavioral abnormalities (Chen and Hong, 2018). Indeed, inborn social behaviors related to sex, defense and maternal care are elicited by sensory input that is processed by the central nervous system to promote successful reproduction (Sokolowski and Corbin, 2012).

From the hundreds of genes essential for neuroendocrine/gonadal control over gametogenesis and fertilization (Matzuk and Lamb, 2008), neurotransmission genes that govern sensory neuron-stimulated social behavior mediate the primary signals that initiate reproduction (Petrulis, 2013a, b; Sokolowski and Corbin, 2012). Social responses such as pleasure, attraction, fear, aggression and avoidance that affect reproduction are processed by the limbic system to modulate motivational responses (Berridge and Kringelbach, 2015; Chen and Hong, 2018). Innate reproductive behaviors are driven by afferent sensory neurons that innervate the limbic system in mammals and are driven by sex and sex hormones (estrogen and testosterone) (Petrulis, 2013a, b). Abnormalities in the cortico-limbic networks that integrate survival-driven reproductive behavior with emotional awareness and memory play crucial roles in the etiology of human “affective disorders”, including depression, bipolar disorder, autism, anxiety and addiction, and represent neurological health conditions (Coria-Avila et al., 2014; Maclean, 1952; Phelps and LeDoux, 2005).

In this study, we aimed to identify novel genes required for reproduction. Our intention was to reach out from the circle of obvious candidates and uncover novel layers of reproductive biology, remaining as open as possible to finding the unexpected. Therefore, instead of taking a targeted approach, we chose an unbiased, forward mutagenesis strategy to identify new genes that impact reproduction using the rat model.

Rats are highly fecund mammals and display robust appetitive and consummatory reproductive behavior (Giordano et al., 1998; Santoru et al., 2014). In rats, sensory input to the limbic system that drives reproduction is mediated predominantly via the olfactory system [olfactory epithelia > olfactory nuclei > main and/or accessory olfactory bulb > medial amygdala > bed nucleus of

stria terminalis > medial pre-optic hypothalamic nucleus and ventromedial hypothalamus](Sokolowski and Corbin, 2012). Pheromones that signal mating bind to chemosensory olfactory receptors in the olfactory epithelium to elicit pre-copulatory social behaviors such as partner investigation, grooming and courtship (Petrulis, 2013a, b; Sokolowski and Corbin, 2012). Pre-copulatory chemosensory signals further culminate in copulatory and post-copulatory behavior that enable fertilization (Petrulis, 2013a, b; Sokolowski and Corbin, 2012). Notably, the rat's olfactory epithelium is uniquely endowed with ~1,400 genes encoding olfactory receptors (Gibbs et al., 2004) and has long provided an experimental system to study mechanisms by which sensory input stimulates social behavior responses that affect reproduction (Petrulis, 2013a, b; Sokolowski and Corbin, 2012).

Sleeping Beauty genetrap insertions occur randomly (Ivics et al., 1997; Izsvak et al., 2000). We previously reported on the production of recombinant spermatogonial stem cell libraries harboring *Sleeping Beauty* genetrap insertions for large-scale production of novel mutant rat strains to perform forward genetic assays (Izsvak et al., 2010). In the current study, a panel of *Sleeping Beauty* mutant rat strains derived from a spermatogonial genetrap library were tested in a forward genetic screen for impaired reproductive behavior phenotypes. In addition to genes required for gamete and embryo development, our screen unveiled new genetic connections between reproduction, fitness and social behavior. Among the reproduction genes, we identified *Atg13*, which has generally been connected to longevity in species ranging from yeast to plants and humans. We also identified *Pclo*-deficient phenotypes that model humans diagnosed with affective disorders and central atrophy (Ahmed et al., 2015; Choi et al., 2011; Sullivan et al., 2009). By combining gene profiling with forward genetics in rats, we further annotated Pclo as a candidate reproductive factor that integrates physiological state with social behavior.

Results

A set of mutations affects reproduction

To identify reproductive genes, we used a forward genetics approach in mutant rats that were produced from a spermatogonial library of *Sleeping Beauty* genetrap mutations (*Figure 1A*). Individual mutant rat strains harbored a *Sleeping Beauty* genetrap insertion within distinct protein coding genes (*Figure 1B and Figure 1 - Source data 1*). A subset of *Sleeping Beauty* genetrap (gt) mutant strains were analyzed for their ability to reproduce after pairing with wildtype (wt) breeders (*Figure 2A and Figure 2 - Source data 1*). Inability to reproduce was linked to a variety of phenotypes that included gametogenesis defects (*Btrc*$^{gt/gt}$, *Ube2k*$^{gt/gt}$, *Pan3*$^{gt/gt}$, *Spaca6*$^{gt/gt}$), embryonic lethality (*Alk3*$^{gt/gt}$, *Exoc6b*$^{gt/gt}$, *Slc1a3*$^{gt/gt}$, *Tmx4*$^{gt/gt}$, *Zmynd8*$^{gt/gt}$), end-stage organ failure (*Atg13*$^{gt/gt}$) and impaired behavior (*Pclo*$^{gt/gt}$, *Dlg1*$^{wt/gt}$) (*Figure 2 - Source data 2 and 3 contain full phenotyping summary*). In total, 12 of 18 mutant genes analyzed (n=17 gene traps + n=1 untrapped gene; *Figure 1B*) proved to be essential for reproduction (*Figure 2A*).

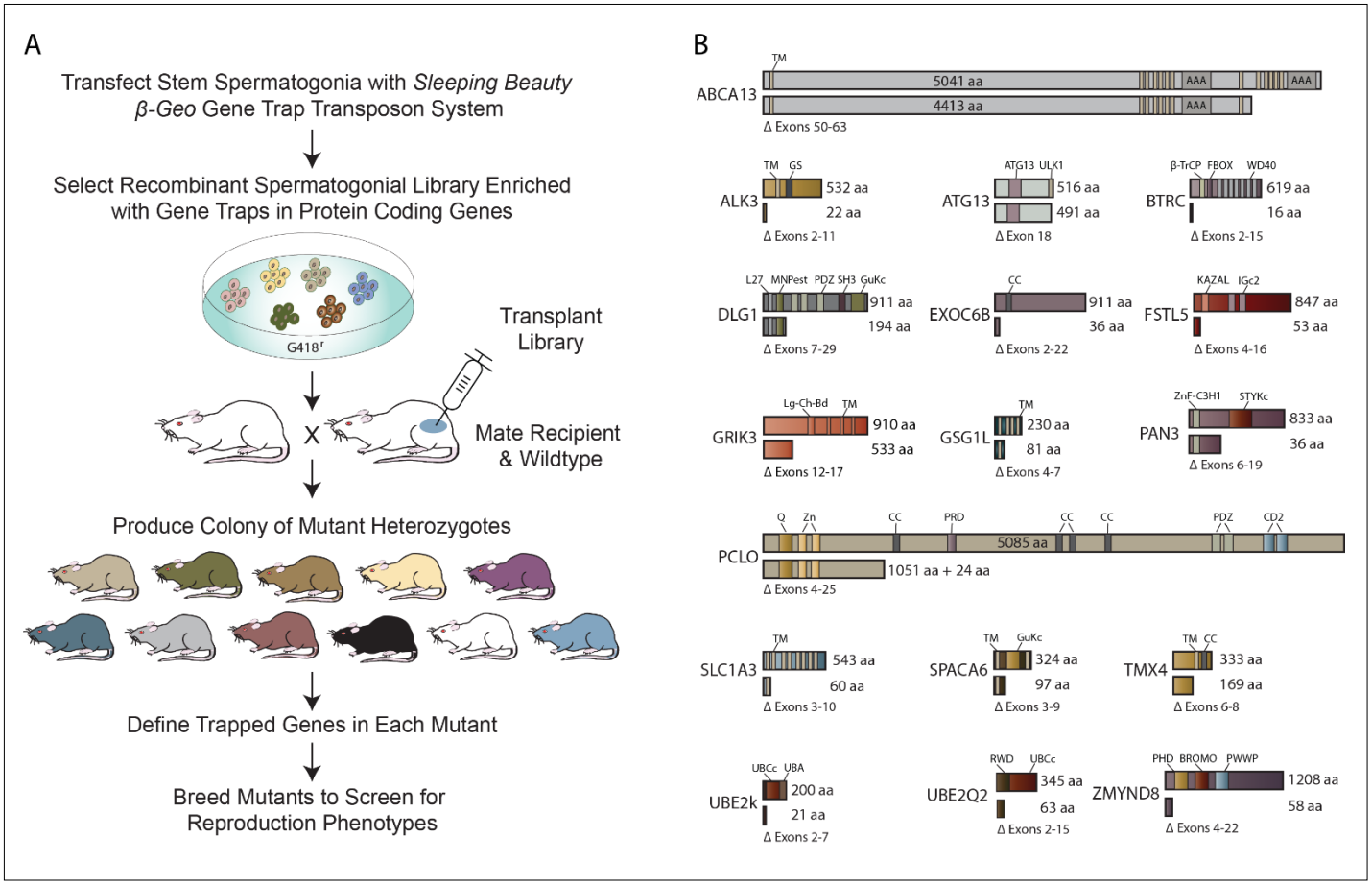

Figure 1. Sperm Stem Cell Based Forward Screen for Rat Reproduction Genes

(**A**) Recombinant rat spermatogonial stem cell libraries are produced by *Sleeping Beauty* transposon genomic insertion. Spermatogonial libraries of randomly inserted *Sleeping Beauty* genetrap mutations are used to produce colonies of mutant rats. Novel *Sleeping Beauty* mutant rat strains are crossed to identify genes that impact reproduction.

Figure 1 continued on next page

Figure 1 continued

In the current study, eleven homozygous mutant rat strains generated were viable following birth (~70%), 6 were embryonic lethal (~28%) and 1 was scored as sub-viable postnatally (~6%). (n=18 mutant rat strains analyzed for ability to reproduce). Similar relative percentages were reported in mice by the European Conditional Mouse Mutagenesis Program (EUCOMM) and the Knockout Mouse Project (KOMP) (Ayadi et al., 2012).

(**B**) Predicted proteins produced in *Sleeping Beauty β-geo* genetrap rat strains (Izsvak et al., 2010). Exon sequences predicted to be excluded (Δ) from mRNAs encoding truncated polypeptides (aa) generated by imposed splicing to the genetrap transposon are shown below respective wildtype proteins for 17 of the 18 mutant rat strains screened for effects on reproduction. An additional transposon insertion within intron 2 of *Rgs22* is *not shown* and is not predicted to truncate the Rgs22 open reading frame due to its intronic genetrap cassette inserting in the 3' to 5' orientation (i.e. untrapped gene). See: *Figure 1 - Source data 1* for full amino acid sequences of the 17 predicted truncated proteins encoded by respective trapped genes, which contain additional epitopes of either 3, 24 or 1319 (β-GEO) amino acids derived from the genetrap construct.

TM, Transmembrane domain; AAA, ATPase Associated with a variety of cellular activities; GS, GS Motif; L27, domain in receptor targeting proteins Lin-2 and Lin-7; MN-PEST, Polyubiquitination (PEST) N-terminal domain of MAGUK; PDZ, Domain present in PSD-95; β-TrCP, D domain of beta-TrCP; FBOX, A Receptor for Ubiquitination Targets; Dlg, and ZO-1/2; SH3, Src homology 3 domain; GuKc, Guanylate kinase homologue; CC, coil coil region; KAZAL, Kazal type serine protease inhibitors; IGc2, Immunoglobulin C-2 Type; Lg-Ch-Bd, Ligated ion channel L-glutamate- and glycine-binding site; ZnF_C3H1, Zinc Finger Domain; STYKc, Protein kinase; unclassified specificity; C2, Protein kinase C conserved region 2 (CalB); UBCc, Ubiquitin-conjugating enzyme E2, catalytic domain homologue; UBA, Ubiquitin associated domain; RWD, domain in RING finger and WD repeat containing proteins and DEXDc-like helicases subfamily related to the UBCc domain; PHD, PHD zinc finger; BROMO, bromo domain; PWWP, domain with conserved PWWP motif.

Mutations that disrupt distinct steps in rat spermatogenesis

Homozygous genetrap mutations in *Btrc*, *Ube2k* and *Pan3* blocked spermatogenesis at pre-meiotic, meiotic and post-meiotic steps, respectively (*Figure 2B; Figure 2 – Figure supplement 1A and 1B*). Only residual numbers of malformed spermatozoa were detected in *Btrc*$^{gt/gt}$ males, and no epididymal spermatozoa were observed in *Ube2k*$^{gt/gt}$ or *Pan3*$^{gt/gt}$ males (*Figure 2C*). In corresponding *Ube2k*$^{gt/gt}$, *Btrc*$^{gt/gt}$ and *Pan3*$^{gt/gt}$ genotypes, spermatogenic arrest was reflected by reduced testis size (*Figure 2D and Figure 2 - Source data 2*).

A group of mutant rats develop gametes, but do not reproduce

Rats with homozygous mutations in the *Spaca6, Atg13* and *Pclo* genes produced both eggs and sperm (*Figure 2C and Figure 2 – Figure supplement 1C*). However, neither sex of *Atg13*$^{gt/gt}$ and *Pclo*$^{gt/gt}$ rats were able to reproduce, as was the case with *Spaca6*$^{gt/gt}$ males (*Figure 2A and Figure 2 – Source Data 1*). *Spaca6*$^{gt/gt}$ females produced relatively normal sized litters when paired with wt males (*Figure 2A and Figure 2 – Source Data 1*). While *Spaca6*$^{gt/gt}$ epididymides had slightly reduced numbers of spermatozoa (*Figure 2C*), their moderate deviation in sperm counts could not explain the infertility phenotype we observed.

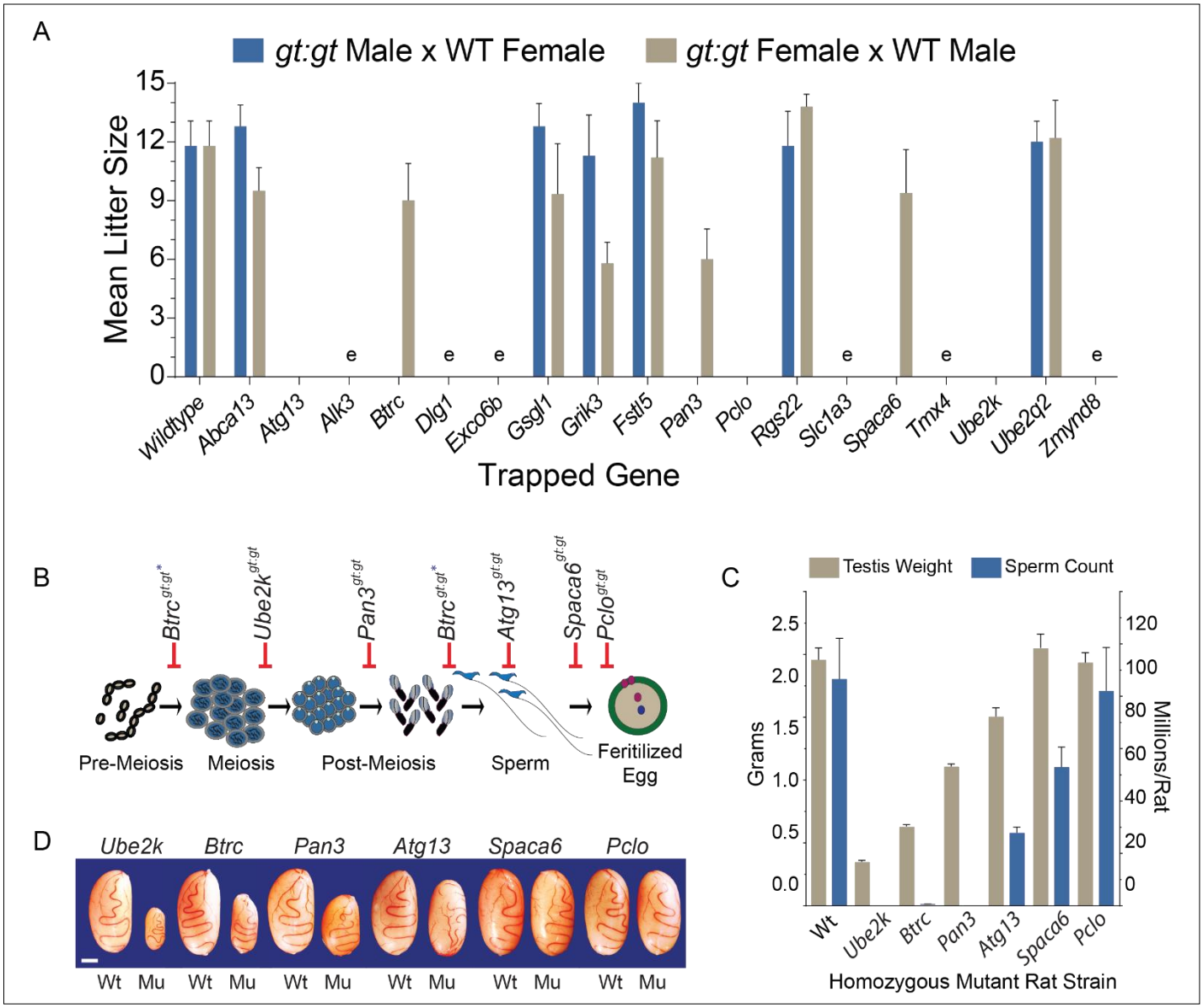

Figure 2. Gene Mutations that Cause Infertility in Rats

(**A**) Mean litter size produced by crossing female and male homozygous *Sleeping Beauty* mutant rats (*gt:gt*) with wildtype breeders (WT). e = embryonic lethal. See detail results on breeding homozygous mutant rat strains in *Figure 1 – Source data 1*.

(**B**) Developmental steps during sperm maturation or fertilization disrupted by respective homozygous genetrap mutations (*gt:gt*) in rats. *Note: *Btrc*$^{gt/gt}$ rats displayed pre-meiotic (~85% tubules) and post-meiotic (~15% tubules) spermatogenic arrest based on co-labeling with nuclear markers (γH2AX and Hoechst 43332 dye).

(**C**) Mean testis weight (tan bars; left y-axis) and epididymal sperm counts (blue bars; right y-axis) from respective homozygous mutant rat strains (±SEM, n=4-6 rats/strain). Measurements taken between postnatal days 120-180. Caudal epididymal spermatozoa from *Spaca6*$^{gt/gt}$ (n=6) and *Pclo*$^{gt/gt}$ (n=4) rats displayed similar basal activity compared to wildtype.

(**D**) Testes from wildtype (Wt) and homozygous genetrap mutants (Mu). Scale bar, 5 mm

The following supplements are available for figure 2:

Figure supplement 1. Gametogenesis defects in rats with gene-trap mutations

Source Data 1. Reproduction phenotypes in rats with gene-trap mutations

Source Data 2. Body, testis and epididymal weight ratio in rats with gene-trap mutations

Source Data 3. Mutant rat phenotypes in current study compared across species

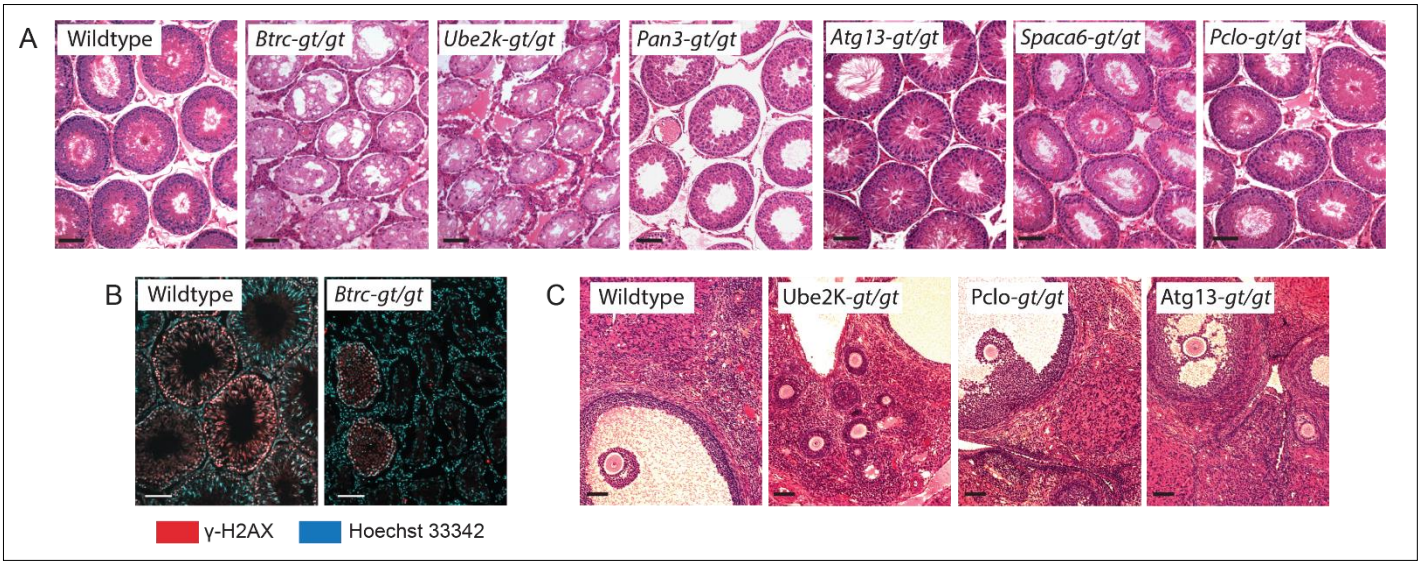

Figure 2 - Figure Supplement 1. Gametogenesis defects in rats with gene-trap mutations
(**A**) H&E stained testis sections from wildtype and respective homozygous genetrap mutant rats. Scale bar, 100 µm.
(**B**) Immunofluorescence labeling of cells in wildtype and mutant *Btrc*$^{gt/gt}$ rat testis sections using an antibody to γH2AX and Hoechst 43332 dye as nuclear markers. Scale bar, 100 µm.
(**C**) H&E stained ovarian sections from wildtype and respective homozygous genetrap mutant rats. Scale bar, 100 µm.

Furthermore, mating behavior appeared normal in *Spaca6*$^{gt/gt}$ males when compared to wt males, as supported by the presence of spermatozoa in vaginal swabs (n=4 breeder pairs). Accordingly, in mutant mice lacking an ~11kb region of chromosome 17, *Spaca6* was initially implicated in gamete membrane fusion (Lorenzetti et al., 2014). As with *Spaca6*$^{gt/gt}$ males, the inability of *Atg13* and *Pclo* homozygous mutants to reproduce could not be explained by an early blockage of gamete production, and therefore required further analyses.

Reproduction defects in *Atg13* mutants correlate with reduced longevity.

Whereas *Autophagy related 13* (*Atg13*) is required for autophagic flux and reaching an optimal lifespan in plants and animals (*Figure 2 – Source data 3*)(Alers et al., 2014; Funakoshi et al., 1997; Suttangkakul et al., 2011), the role of *Atg13* in additional reproduction-related traits is unknown. All male *Atg13*$^{gt/gt}$ mutants were characterized by reduced testis size and epididymal sperm counts compared to wt (*Figure 2C and 2D*) but had relatively high testis-to-body weight and epididymis-to-body weight ratios (*Figure 2 – Source data 2*). *Atg13*$^{gt/gt}$ cauda epididymal spermatozoa flagella were immotile and displayed more detached heads and tails than WT (n=4/genotype). The insertional mutation resulted in a truncated form of *Atg13* predicted to lack exon 16 (*Atg13*$^{\Delta e16}$) (*Figure 3A*). *Atg* exon 16 encodes the 25 carboxyl-terminal amino acids in Atg13 (*Figure 3A*). Expression of *Atg13*$^{\Delta e16}$ generated a protein that resembled wt ATG13: it was abundant in testes, with lower levels in other tissues (*Figure 3A inset*).

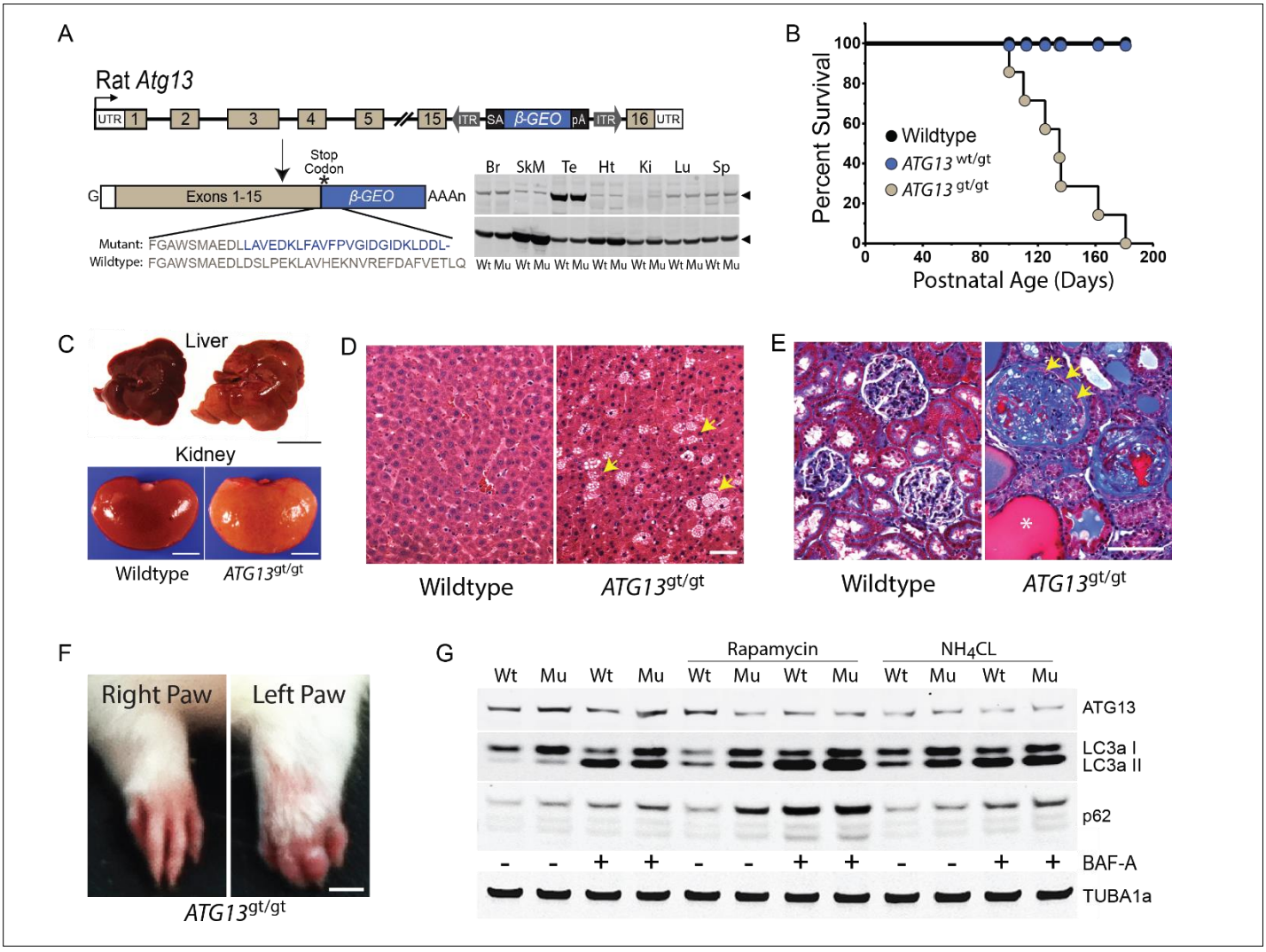

Figure 3. Pathology linked to the COOH-terminal 25 amino acids in rat Autophagy Related 13

(**A**) Diagram of *Sleeping Beauty β-Geo* genetrap in rat *Atg13* intron 15. The genetrap splices to *Atg13* exon 15 and is out of frame with the *β-Geo* reporter that effectively replaces *Atg13* exon 16 (*Atg13*$^{\Delta e16}$). *Atg13* exon 16 encodes the C-terminal 25aa of wildtype Atg13 and is predicted to be replaced by a 24aa epitope (blue font) derived from the genetrap construct, thereby, generating a similar size mutant protein. *Inset*: (top panel) western blot probing ATG13 in tissues from wildtype (WT) and homozygous mutant *Atg13*$^{gt:gt}$ (Mu) rat littermates; (bottom panel) same blot probed for GAPDH. Arrowheads point to WT and Mu rat proteins with molecular size of ATG13 (~65 kDa) and GAPDH (~37 kDa). Br, brain; SkM, skeletal muscle; Te, testis; Ht, heart; Ki, kidney; Lu, lung; Sp, spleen

(**B**) Kaplan-Meier estimator of postnatal survival for *Atg13*$^{wt:wt}$ (wildtype), *Atg13*$^{wt:gt}$ (heterozygous) and *Atg13*$^{gt:gt}$ (homozygous) mutant rats.

(**C**) Liver (top) and Kidney (bottom) from wildtype and homozygous mutant (*Atg13*$^{gt:gt}$) littermates. Liver scale bar, 2 cm; Kidney scale bar 5 mm.

(**D**) Hematoxylin and Eosin stained liver sections in *Atg13*$^{wt:wt}$ and *Atg13*$^{gt:gt}$ rats. Note, fatty liver in *Atg13*$^{gt:gt}$ rats (arrows). Liver sections from littermates, postnatal day 110. Scale bar 50 µm.

(**E**) Trichrome stained sections illustrating dramatic sclerosis of the glomerular tuft and fibrosis in Bowman's capsule of an *Atg13*$^{gt:gt}$ rat. Note proliferating epithelial cells lining Bowman's capsule (arrows). An adjacent tubule is dilated and filled with protein rich filtrate (asterisks). Kidney sections from wildtype and *Atg13*$^{gt:gt}$ littermates, postnatal D110. Scale bar 100 µm.

(**F**) Forearms of *Atg13*$^{gt:gt}$ phenotype in one strain. Note swelling of left arm and digits. Scale bar, 5 mm.

(**G**) Relative expression of the autophagy marker proteins Atg13, LC3a I, LC3a II and p62 compared to TUBA1a (loading control) in embryonic fibroblasts derived from wildtype and mutant rats following treatment with or without combinations of rapamycin, ammonium chloride (NH_4CL) and bafilomycin-A1 (BAF-A)

Notably, all *Atg13*$^{gt/gt}$ rats inherited pathologies associated with premature death at 3-5 months of age (*Figure 3B*). The livers and kidneys of *Atg13*$^{gt/gt}$ rats were abnormal (*Figure 3C*), with the liver containing cells scattered throughout histological sections displaying small spherical vacuoles, consistent with an accumulation of triglycerides (*Figure 3D*). All the kidneys that were examined displayed marked glomerulonephritis and moderate tubule interstitial disease (*Figure 3E*). Homozygous *Atg13*$^{gt/gt}$ animals (n=3) from one of three pedigrees also demonstrated edematous paws and digits in adult animals (*Figure 3F*).

Consistent with *Atg13*'s biological function, changes in the relative abundance of autophagy markers LC3a-I/II and p62 were found in *Atg13*$^{gt/gt}$ embryonic fibroblasts (*Figure 3G*). Rapamycin treatment synergized with *Atg13*$^{gt/gt}$ to increase LC3a-I/II and p62 relative abundance in fibroblasts, implicating Atg13's COOH-terminal peptide in regulating mTorc-dependent autophagy signals (*Figure 3G*). The reproduction defects in both female and male *Atg13*$^{gt/gt}$ rats correlated with adult-lethal pathologies, and in males, *Atg13*$^{gt/gt}$ was further associated with abnormal spermatozoa.

Compromised neurotransmission in *Pclo* mutants

Pclo$^{gt/gt}$ rats harbor the *Sleeping Beauty* genetrap in *Pclo* intron 3, deleting exons 4-25 (*Pclo*$^{SB\Delta 4\text{-}25}$ rats) (*Figure 4A*). *Pclo* encodes multiple protein isoforms (70-560kDa) that are primarily localized in the cytomatrix of pre-synaptic neurons and have been implicated to play a key role in synaptic transmission (Cases-Langhoff et al., 1996). Piccolo is expressed in various tissues and is enriched in the brain, where it is relatively abundant in the cerebellum, pituitary gland, cortex, hypothalamus and nucleus accumbens (GTEX Portal PCLO). Despite their reproductive failure (*Figure 2A*), *Pclo*$^{gt/gt}$ mutant rats did not display any obvious dysfunction during gametogenesis (*Figure 2 – Figure supplement 1A and 1C*). Numbers of epididymal spermatozoa from *Pclo*$^{gt/gt}$ rats were relatively normal (*Figure 2C*). However, spermatozoa from *Pclo*$^{gt/gt}$ rats were not found in vaginal swabs of WT females (6 of 6 breeder pairs) (*Figure 4B*), and spermatozoa from WT males were not detected in *Pclo*$^{gt/gt}$ females (6 of 6 breeder pairs) (*Figure 4B*). We took these findings alongside the known predominant distribution of *Pclo* transcripts in the brain and hypothesized that reproductive failure in *Pclo*$^{gt/gt}$ rats was caused by neurological abnormalities.

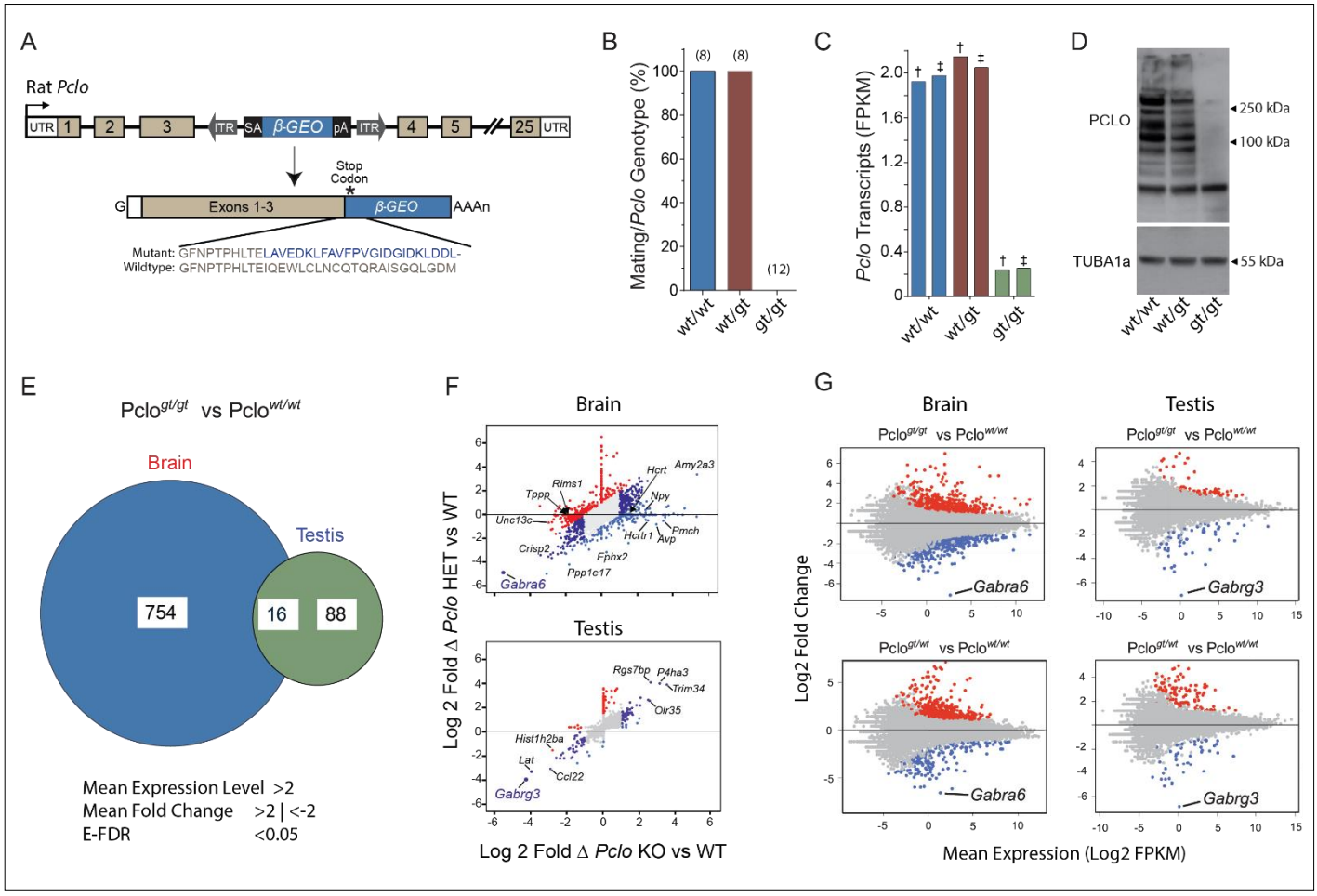

Figure 4. RNA profiling in mutant *Piccolo* rats

(**A**) Diagram of *Sleeping Beauty β-Geo* genetrap in rat *Pclo* intron 3. The genetrap splices to *Pclo* exon 3, out of frame with the *β-Geo* reporter. The genetrap is predicted to replace the C-terminal 3805aa or 4010aa encoded by exons 4-25 of respective wildtype *Pclo* isoforms with a 24aa construct-derived epitope (blue font) to generate $Pclo^{\Delta e4\text{-}25}$.

(**B**) $Pclo^{wt:wt}$, $Pclo^{wt:gt}$ and $Pclo^{gt:gt}$ rat mating after pairing with wildtype breeders based on identification of spermatozoa in vaginal swabs. (n) = 8 to 12 total breeder pairs/genotype, or 4 to 6 breeder pairs/sex/genotype for $Pclo^{wt:gt}$ and $Pclo^{gt:gt}$ mutant strains.

(**C**) Relative abundance (FPKM values) of *Pclo* transcript isoforms in $Pclo^{wt:wt}$, $Pclo^{wt:gt}$ and $Pclo^{gt:gt}$ rat brains. †NM_020098, encodes the full length 4880-amino acid isoform; ‡NM_001110797, encodes the full length 5041-amino acid isoform.

(**D**) Western blot of Piccolo isoforms and TUBA1a in total brain lysates prepared from $Pclo^{wt:wt}$, $Pclo^{wt:gt}$ and $Pclo^{gt:gt}$ rats.

(**E**) Venn diagram shows the number of differentially expressed genes (DEGs) in the brain (754) and testis (88) or genes commonly expressed in both tissues (16) of $Pclo^{gt/gt}$ rats compared to $Pclo^{wt/wt}$ rats.

(**F**) Relative abundance of DEGs in $Pclo^{wt/gt}$ (HET) and $Pclo^{gt/gt}$ (KO) rat brain (top) and testis (bottom) vs wildtype (WT). DEGs that changed more in HET or more in KO vs WT are shown in red and light blue, respectively (log2-fold change >1 or <-1; FDR < 0.05). Genes that changed comparably in abundance in both HET and KO but were differentially expressed relative to WT are shown in dark blue (log2-fold change >1 or <-1; FDR < 0.05). Note, that the *Pclo* mutation affected more changes in the brain vs testis transcriptome.

(**G**) Fold change in relative brain (left) and testis (right) transcript abundance (Log2 FPKM values) in $Pclo^{wt/gt}$ and $Pclo^{gt/gt}$ rats vs $Pclo^{wt/wt}$ rats. DEGs are shown in red (increased abundance) and blue (decreased abundance), respectively (log2-fold change >1 or <-1; FDR < 0.05). Note, the decreased *Gabra6* and *Gabra3* abundance in brain and testis, respectively, in both $Pclo^{wt/gt}$ and $Pclo^{gt/gt}$ rats.

The following source data are available for figure 4:

Source data 1. Fragments per kilobase of transcript per million mapped reads (FPKM) in $Pclo^{wt/wt}$, $Pclo^{wt/gt}$ and $Pclo^{gt/gt}$ rat brains and testes.

201

To gain insights into Piccolo's role in reproductive phenotypes, RNA sequencing (RNA-seq) was carried out on testes and brain tissues from *Pclo*$^{gt/gt}$, *Pclo*$^{gt/wt}$ and *Pclo*$^{wt/wt}$ animals (~6 mo old). *Pclo* transcripts are readily detectable in the brain (*Figure 4C*), whereas the testicular expression of *Pclo* is low (< 0.1 FPKM) (*Figure 4 – Source data 1*). In the brain, the genetrap insertion reduced *Pclo* expression to the point that it was undetectable (< 0.1 FPKM) in homozygous *Pclo*$^{gt/gt}$ rats (*Figure 4C*), while no significant transcriptional changes of *Pclo* could be detected in heterozygous *Pclo*$^{wt/gt}$ rats (*Figure 4C*). Similarly, at the protein level, Pclo was reduced by >99% in the brains of *Pclo*$^{gt/gt}$ rats, but Pclo was not significantly affected in *Pclo*$^{wt/gt}$ compared to *Pclo*$^{wt/wt}$ littermates (*Figure 4D*). Thus, expression from a single *Pclo* allele appears to drive relatively normal levels of the gene product, and the phenotype that was observed appears to be connected to the allelic origin of Piccolo.

Our transcriptome analysis of *Pclo*$^{gt/gt}$ and *Pclo*$^{wt/wt}$ rats revealed a higher number of differentially expressed genes (DEGs) in the brain (754) than testis (88), while 16 genes were affected in both tissues (FPKM > 2 and log2 fold change |1| and E-FDR < 0.01) (*Figure 4E and Figure 4 - Source data 1*). Inclusive to the 16 DEGs that were affected in both brain and testes, *Tspo*, *Ces1d*, *Folr1* and *Adh1* (*Figure 4E and Figure 4 - Source data 1*) regulate steroid hormone/vitamin biosynthesis, signaling and transport in the blood stream (Lian et al., 2019; Rupprecht et al., 2010; Spiegelstein et al., 2004; Yang et al., 2018). Despite similar Piccolo RNA/protein abundance in *Pclo*$^{wt/wt}$ and *Pclo*$^{wt/gt}$ rat brains, 325 genes were differentially expressed (log2FC |1|) in the brains of heterozygotes compared to wildtype or homozygotes (*Figure 4F and Figure 4 - Source data 1*), reflecting robust allelic effects. The most significantly affected genes in both *Pclo*$^{gt/gt}$ and *Pclo*$^{wt/gt}$ rats were *Gabra6 (GABA(A) Receptor Subunit Alpha 6)* in the brain and *Gabrg3 (GABA(A) Receptor Subunit Gamma-3)* in the testis (*Figure 4G – Figure 4 - Source data 1*).

Consistent with our hypothesis that lack of reproduction by *Pclo*$^{gt/gt}$ rats was caused by a neurological defect, Gene Ontology (GO) analyses revealed the most significantly down-regulated processes in *Pclo*$^{gt/gt}$ vs *Pclo*$^{wt/wt}$ rats included *Synaptic Transmission* and *Neurogenesis* gene sets (p<0.000006; *Figure 5 - Source data 1*). A prominent cluster of 80 downregulated *Synaptic Transmission* genes in the brain (*Figure 5A*) included the *gamma-aminobutyric acid (GABA) signaling pathway* (GO:0007214, p=0.0000009) (*Figure 5B and Figure 5 - Source data 1*). While *Gabra6* is abundantly expressed in the cerebellum of the brain (GTEX Portal Gabra6, FPKM

234 >1), *Gabrg3* has a higher enrichment in the testis and a moderate enrichment in the pituitary

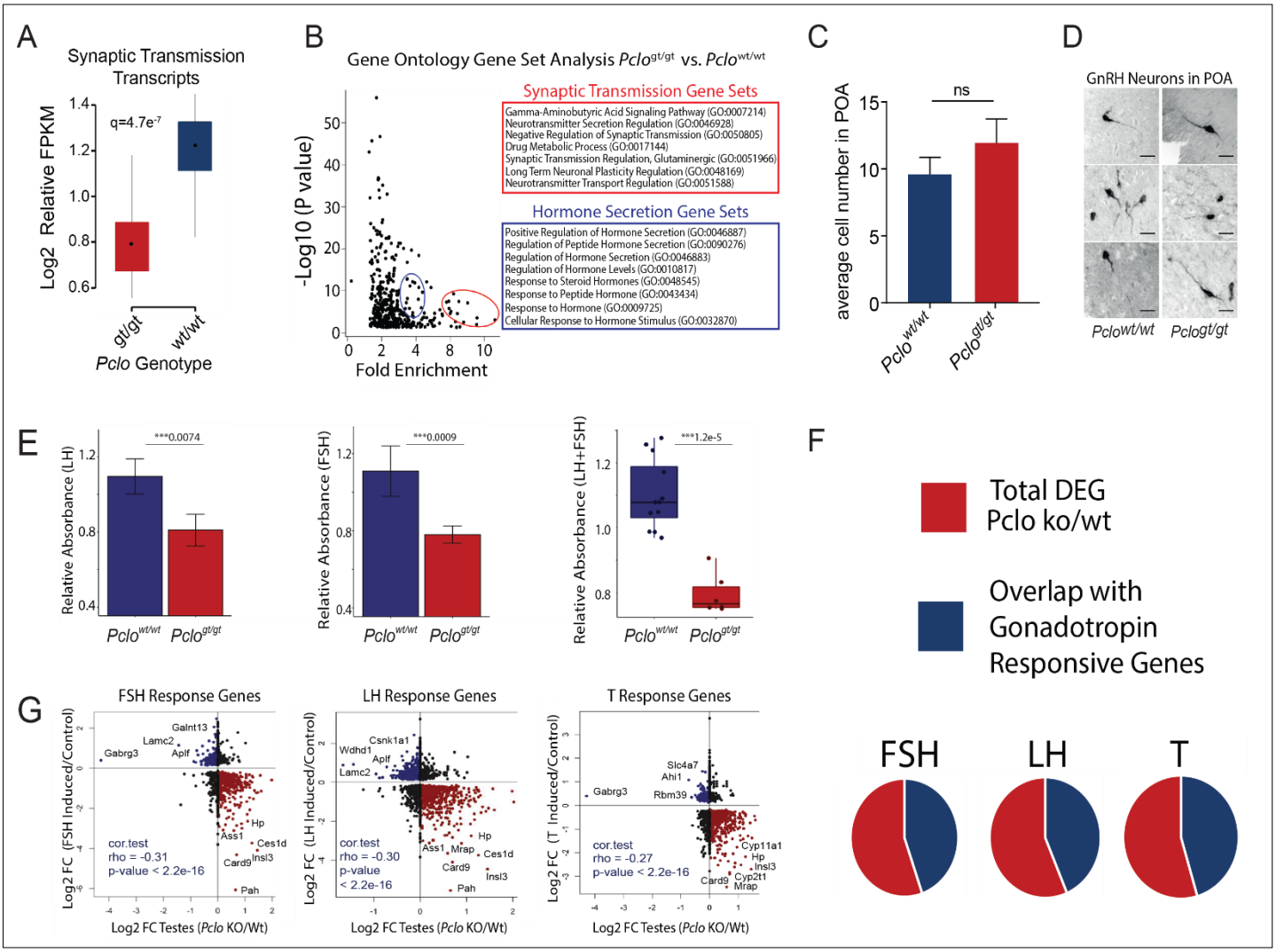

Figure 5. Piccolo deficiency disrupts synaptic transmission and gonadotropin responsive gene sets

(**A**) Ontology of DEGs in *Pclo*$^{gt/gt}$ vs *Pclo*$^{gt/gt}$ rat brains. Mean relative abundance of 80 synaptic transmission GO genes in *Pclo*$^{gt/gt}$ vs *Pclo*$^{wt/wt}$ rat brains (log2-fold change >1 or <-1; FDR < 0.05).

(**B**) Gene Ontology gene enrichment pathway cluster analysis in *Pclo*$^{wt/wt}$ vs *Pclo*$^{gt/gt}$ rat brains identified misregulated clusters for Hormonal Secretion (blue circle & box) and Synaptic Transmission (Red Circle & box) GO gene sets.

(**C**) Quantification of the average number of GnRH positive neurons per section within the POA, revealing that *Pclo*-deficiency does not affect the number of GnRH neurons within the preoptic area (POA).

(**D**) High magnification images of GnRH positive neurons in *Pclo*$^{wt/wt}$ vs *Pclo*$^{gt/gt}$ rat brains (Scale bars = 10 µm).

(**E**) Bar plots demonstrate relative FSH (left) and LH (center) concentrations in *Pclo*$^{wt/wt}$ and *Pclo*$^{gt/gt}$ rats determined by ELISA at two dilutions (5x and 10x) and three technical replicates. ELISA mean ±SD absorbance values obtained from three animals (two *Pclo*$^{wt/wt}$ and one *Pclo*$^{gt/gt}$). Asterisks represent p-values obtained by t-test. Boxplot with jitters (right) is an alternative representation of LH and FSH levels analyzed together between *Pclo*$^{wt/wt}$ vs *Pclo*$^{gt/gt}$ rats. Asterisks represent p-values obtained by Wilcox test. Each dot represents a replicate (biological/technical).

(**F**) Overlap between DEGs in *Pclo*$^{gt/gt}$ rat testes and genes regulated by gonadotropins in rat testes(Zhou et al., 2010); FSH, Follicle Stimulating Hormone; LH, Luteinizing Hormone, T, Testosterone (log2-fold change >1 or <-1; FDR < 0.05).

(**G**) Scatter plots of DEGs in *Pclo*$^{gt/gt}$ rat testes and genes regulated by gonadotropins in rat testes (Zhou et al., 2010).

The following supplements and source data are available for figure 5:

Source data 1. Gene ontology analyses from *Pclo*$^{wt/wt}$, *Pclo*$^{wt/gt}$ and *Pclo*$^{gt/gt}$ rat brains and testes

Figure supplement 1: Gene ontology analyses on GnRH pathway in mutant *Pclo* rats.

Figure supplement 2: Misregulated gene networks downstream of GnRH signaling in mutant *Pclo* rats.

gland and hypothalamus (GTEX Portal Gabrg3, FPKM>1). Curiously, the expression of both, *Gabra6* in brain, and *Gabrg3* in testes, dropped to undetectable levels (FPKM < 0.01) in *Pclo*$^{wt/gt}$ and *Pclo*$^{gt/wt}$ rats, suggesting a dominant phenotype in *Pclo*$^{SB\Delta4\text{-}25}$ mutants that results in a close-to KO phenotype for each GABA(A) receptor subunit in respective tissues (*Figure 4G and Figure 4 - Source data 1*).

Disturbed hormonal secretion in *Pclo* mutants

In addition to downregulated *Synaptic Transmission* gene sets (*Figure 5A*), Gene Ontology analysis on *Pclo*$^{gt/gt}$ rat brains revealed a prominent cluster of *Hormonal Secretion* gene sets that were downregulated compared to *Pclo*$^{wt/wt}$ animals (*Figure 5B*). Further pathway analyses (PANTHER) revealed that genes affected by the gene trapped *Pclo*$^{SB\Delta4\text{-}25}$ fall most frequently into major signaling pathways of the *Gonadotropin-releasing hormone (GnRH) receptor,* followed by *Wnt*, *Chemokine-cytokine* and *CCKR* signaling (*Figure 5 – figure supplement 1A*). Notably, signaling pathways coupled to the *Gonadotropin-releasing hormone (GnRH) receptor* gene set control the hypothalamic-pituitary-gonadal axis that is critical for gamete development (Carmel et al., 1976) and that has been implicated in regulating reproductive behavior (Boehm et al., 2005; Yoon et al., 2005).

Notably, excitatory GABA neurons function to activate GnRH neurons (Watanabe et al., 2014), and GABA signaling via GABA receptors is known to affect the rate of GnRH synthesis and pattern of GnRH release (Herbison and Moenter, 2011). The GABA signal, which depolarizes GnRH neurons during development, also regulates overall GnRH neuron maturation (e.g. migration to the brain). GABA(A) receptor subunits are differentially expressed during the process of GnRH-1 maturation (Temple and Wray, 2005) and Gabra6 is a receptor subunit within embryonic GnRH-1 neurons that is replaced by Gabra2 during adult life (Temple and Wray, 2005). Thus, the reported Gabra6-positive GnRH neuronal progenitors led us to wonder whether the close-to-KO *Gabra6* phenotype in *Pclo*$^{gt/gt}$ rats altered GnRH neuron migration patterns during development, and in turn, compromised establishment of proper GnRH receptor signaling.

A direct assessment of GnRH neurons in the brains of adult *Pclo*$^{gt/gt}$ rats revealed normal numbers of GnRH immuno-positive cells in the pre-optic area of the hypothalamus that projected normally

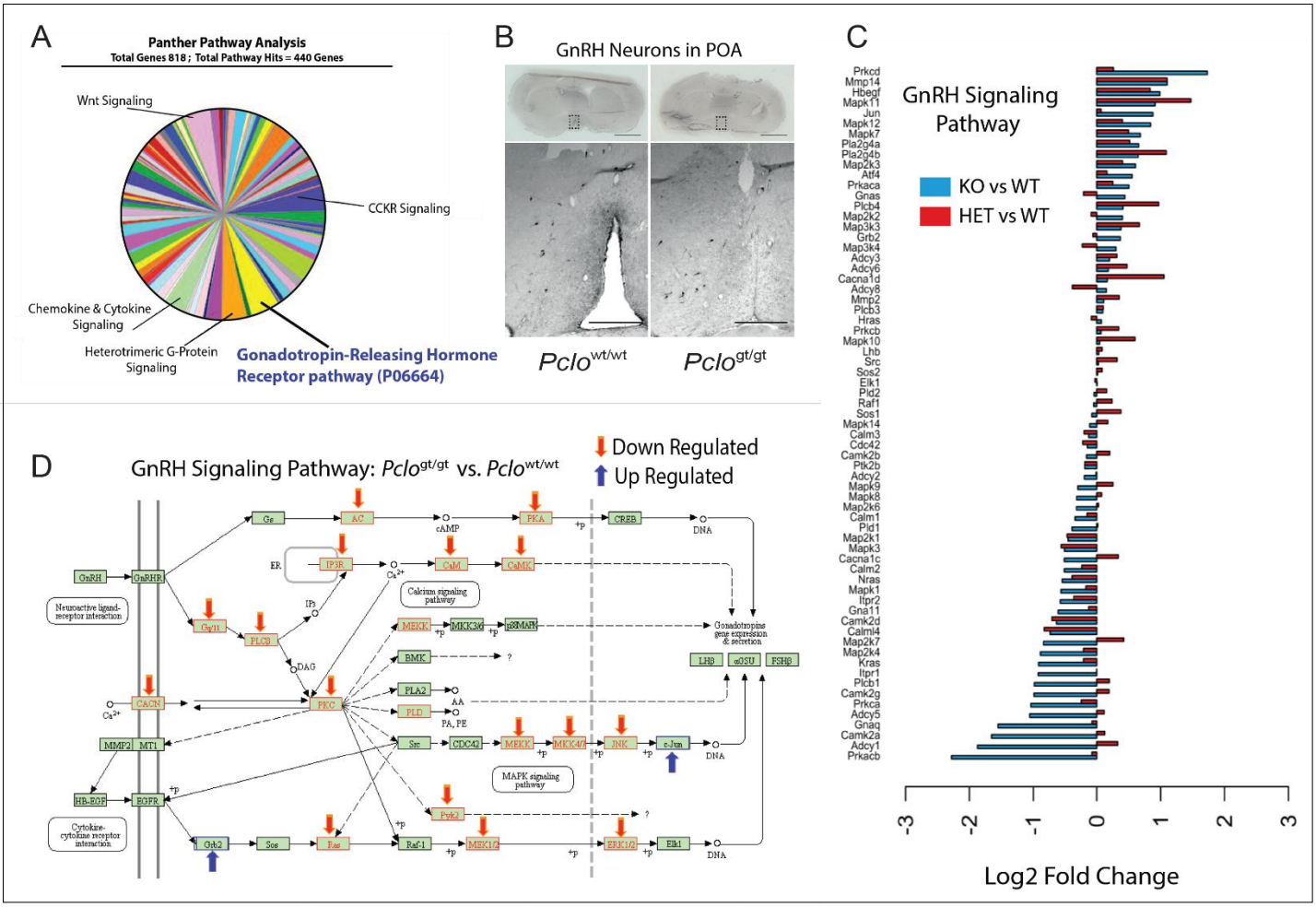

Figure 5 – Figure supplement 1. Gonadotropin Releasing Hormone (GnRH) signaling pathway genes are downregulated in the brain of mutant *Piccolo* rats.

(**A**) Panther Pathway finder analysis on down regulated Hormonal Secretion GO: gene sets identify GnRH signaling pathway as the prominent cluster of DEGs in *Pclo*$^{gt/gt}$ vs *Pclo*$^{wt/wt}$ rat brains.

(**B**) Coronal brain sections from Pclo$^{wt/wt}$ or Pclo$^{gt/gt}$ postnatal day 100 rat brains immuno-stained with GnRH antibodies. Lower panel, 5x magnification of the preoptic area (POA) located in the boxed area reveal presence of somata and GnRH positive neuron processes flanking the third ventricle. Scale bars = upper panel 0.3 cm, lower panel 1000 µm.

(**C**) Relative abundance of GnRH signaling pathway GO: gene set in *Pclo*$^{gt/gt}$ (KO) and *Pclo*$^{wt/gt}$ (HET) vs *Pclo*$^{wt/wt}$ (WT) rat brains.

(**D**) KEGG pathway analysis predicts downregulated GnRH signaling pathways in *Pclo*$^{gt/gt}$ rat brains vs *Pclo*$^{wt/wt}$ rat brains. *Note*: See Panel C for official GnRH signaling pathway gene symbols; KEGG pathway analysis illustrates common gene acronyms.

into the medial eminence (*Figure 5C and 5D; Figure 5 – figure Supplement 1B*). Thus, GnRH neuron development within the pre-optic area of *Pclo*$^{SB\Delta4\text{-}25}$ rats did not appear to be affected by reduced *Gabra6* expression, suggesting that other signaling mechanisms might compensate for *Gabra6* function during the process of GnRH neuron maturation. Mapping differentially expressed genes in the brains of *Pclo*$^{gt/gt}$ rats on the KEGG database revealed that several components of the GnRH signaling pathway were in fact downregulated compared to *Pclo*$^{wt/wt}$ rats (*Figure 5 – Figure Supplement 1C and 1D*).

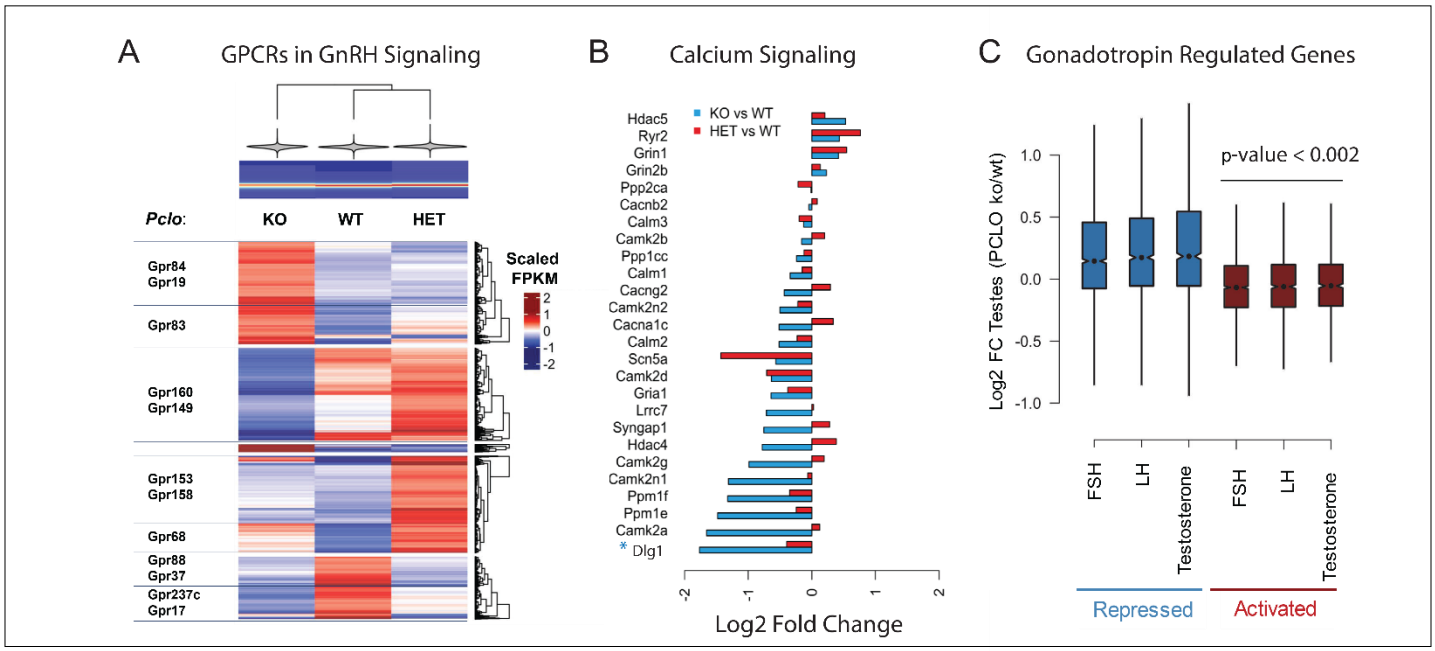

Figure 5 – Figure supplement 2. Misregulated gene networks downstream of GnRH signaling.
(**A**) Relative abundance of DEGs encoding G-Protein Coupled Receptors (GPCRs) involved in conducting GnRH signaling on gonadotropes GO: gene set components in *Pclo*$^{gt/gt}$ (KO) and *Pclo*$^{wt/gt}$ (Het) vs *Pclo*$^{wt/wt}$ (WT) rat brains.
(**B**) Relative abundance of Calcium Signaling GO: gene set components in *Pclo* KO and HET vs WT rat brains. *Note, *Dlg*$^{wt/gt}$ mutant rats displayed altered behavior and reduced fecundity (*Figure 2 - Source data 3*).
(**C**) Relative abundance of Gonadotropin Regulated Genes in *Pclo* KO vs WT rat testes (PCLO ko/wt) that are Repressed or Activated by FSH, Follicle Stimulating Hormone; LH, Luteinizing Hormone, T, Testosterone (Zhou et al., 2010).

The GnRH receptor transmits its signals predominantly through *Heterotrimeric G-proteins*, a category that is also significantly affected in *Pclo* mutants (*Figure 5 – figure supplement 1A*). Our analysis revealed that a major fraction of the G-protein coupled receptors (GPCRs) involved in conducting GnRH signaling on gonadotrophs are differentially enriched in the brains of *Pclo* $^{gt/gt}$ rats compared to *Pclo*$^{wt/gt}$ and *Pclo*$^{wt/wt}$ rats (*Figure 5 – figure supplement 2A*). Similarly, the cascade involved in mobilizing Ca^{2+} from $InsP_3$-sensitive intracellular pools, required for the secretion of gonadotropins, is impaired in *Pclo*$^{gt/gt}$ rats (*Figure 5 – figure supplement 2B*). Thus, downregulation of GnRH-dependent GPCR- and Ca^{2+}-stimulated processes may well affect end products of the GnRH receptor signaling pathway (e.g. luteinizing hormone, LH; follicle-stimulating hormone, FSH; *Figure 5 – figure supplement 1D*). Indeed, blunted expression of GnRH signaling gene sets corresponded to reduced plasma levels of LH and FSH in the *Pclo* KO compared to WT (*Figure 5E*).

Would the decreased level of gonadotropin hormones affect their target gene expression in the testes of *Pclo*$^{gt/gt}$ rats? To answer, we determined transcript levels of genes that might be

stimulated or repressed by LH and FSH or regulated by testosterone (Zhou et al., 2010) in *Pclo*$^{gt/gt}$ vs *Pclo*$^{wt/wt}$ rats. This analysis revealed that about half of the dysregulated genes in *Pclo*$^{gt/gt}$ testes responded to a particular hormonal stimulation in a reverse order (rho = -0.31 and p-value < 2.2e-^{16}) (*Figure 5F*; *Figure 5 – figure supplement 2C*). *Gabrg3*, *Ces1d*, *Card9*, *Insl3* and *Hp* appeared among the most affected targets of LH, FSH and/or testosterone in *Pclo*$^{gt/gt}$ mutant rat testes (*Figure 5G*). Thus, downregulated neuroendocrine GnRH signaling failed to activate several gonadotropin-responsive target genes in the testis, likely contributing to the *Pclo*-deficient rat's infertility phenotypes.

Pclo deficiency up-regulates hypothalamic genes associated with social behavior

To decipher dysregulated *GnRH receptor signaling* in *Pclo* rats (*Figure 5 – Figure supplement 1A-D*) we further evaluated altered gene signatures in the *Pclo*$^{gt/gt}$ rat brain encoding factors that would function upstream of GnRH signaling pathways to suppress GnRH neuron activity. We identified a set of transcripts encoding neuroendocrine hormones (*Npy*, *Pmch*, *Hcrt1*, *Trh*, *Avp*) that was selectively upregulated in *Pclo*$^{gt/gt}$ rat brains by >3-fold vs wt (*Figure 4F*; *Figure 4 – Source data 1*). *Npy*, *Pmch*, *Hcrt1*, *Trh* and *Avp* are each known to physiologically regulate GnRH-1 neuron activity, energy balance and/or social behavior (Bosch, 2013; Luquet and Magnan, 2009; Piet et al., 2015; True et al., 2011), potentially adding an additional layer to the complexity of the infertility phenotype. Based on up-regulated *hypothalamic polypeptide hormone* and down-regulated *GnRH receptor signaling* gene profiles in Pclo-deficient rats, Piccolo embodies a candidate presynaptic factor that regulates reproductive behavior in response to an organism's physiological state.

Reproductive failure in *Pclo* mutant rats is associated with neurological and behavioral defects

To follow up on altered synaptic transmission gene sets observed in the *Pclo* mutants as well as the potential behavioral aspects of the infertility phenotype, we conducted studies on brain function and behavior. Consistent with dominant GABA(A) endophenotypes (*Figure 4G*), both *Pclo*$^{wt/gt}$ and *Pclo*$^{gt/gt}$ mutations increased mean seizure frequencies (≥8-fold) compared to *Pclo*$^{wt/wt}$ littermates (n=8/genotype) (*Figure 6A, left*). The EEG morphology in *Pclo*$^{wt/gt}$ and *Pclo*$^{gt/gt}$ rats resembled short duration absence-type seizures, displaying a characteristic 6-8 Hz spike-

wave generalized onset (*Figure 6A, right*), with no convulsive activity, and functionally verifying the significance of altered *Synaptic Transmission* gene sets (*Figure 5A and 5B*).

In contrast to their *Pclo*$^{wt/wt}$ littermates (e.g. *Figure 6 - Supplement videos 1 and 2*), female and male *Pclo*$^{gt/gt}$ rats exhibited a relative disinterest in courting the opposite sex upon being introduced into the same cage with *Pclo*$^{wt/wt}$ rats (p=0.0002 compared to WT littermates,

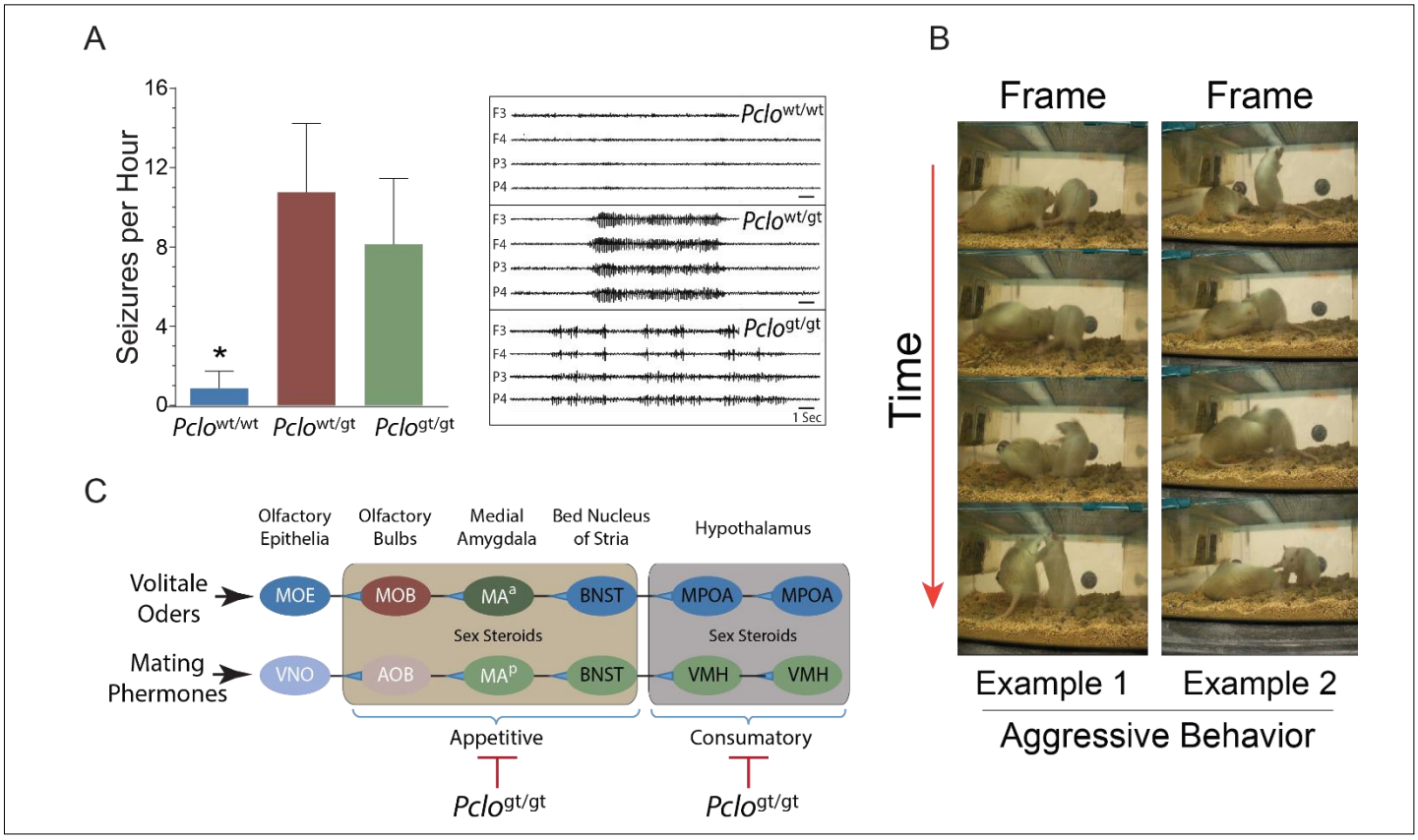

Figure 6. Dominant neurotransmission and recessive reproductive behavior traits in *Pclo* mutant rats.
(**A**) *Left*: Seizure rates recorded in *Pclo*$^{wt:wt}$, *Pclo*$^{wt:gt}$ and *Pclo*$^{gt:gt}$ rats (n=4 rats/genotype). p<0.001 for *Pclo*$^{wt:wt}$ vs. *Pclo*$^{wt:gt}$ or *Pclo*$^{gt:gt}$ rats; p=0.1 for *Pclo*$^{wt:gt}$ vs. *Pclo*$^{gt:gt}$ rats. *Right*: Representative EEG tracings recorded in *Pclo*$^{wt:wt}$, *Pclo*$^{wt:gt}$ and *Pclo*$^{gt:gt}$ rat brains.
(**B**) Altered social behavior in mutant *Pclo* rats. Time lapse frames showing an agitated *Pclo*$^{gt/gt}$ male lunging defensively at a *Pclo*$^{wt/wt}$ female rat. Similar aggressive behavior was not observed in *Pclo*$^{wt/gt}$ or *Pclo*$^{wt/wt}$ rats.
(**C**) Typical social responses to neural connections between the rat olfactory and limbic nervous systems are blocked in *Pclo*$^{gt/gt}$ rats. Normally, pheromones bind olfactory receptors in the rat's olfactory epithelium to elicit pre-copulatory social behaviors including partner investigation, grooming and courtship as essential responses that signal progression to copulatory and post-copulatory behaviors (Sokolowski and Corbin, 2012). Hypothalamic regions innervated by the amygdala and BNST are essential for more downstream pre-copulatory (lordosis), copulatory (mounting, intromission, ejaculation) and post-copulatory (parental care) reproductive behaviors and are effectively modulated by sex hormones (Petrulis, 2013a, b; Sokolowski and Corbin, 2012)

MOE, Medial Preoptic Area; VNO, Vomeronasal Organ; MOB, Main Olfactory Bulb; AOB, Accessory Olfactory Bulb; MAa, Medial Amygdala-anteroventral; MAp Medial Amygdala-posteroventral; BNST, Bed Nucleus of Stria Terminalis; MPOA, Medial Preoptic Area; VMH, Ventromedial Hypothalamus

Figure 6 continued next page

Figure 6 continued

The following supplements and source data are available for figure 6:

Video supplement 1. Typical precopulatory behavior displayed between *Pclo*$^{wt:wt}$ female and *Pclo*$^{wt:wt}$ male rats
Video supplement 2. Typical conspecific social interactions displayed between *Pclo*$^{wt:wt}$ male rats
Video supplement 3. Atypical precopulatory behavior displayed between *Pclo*$^{gt:gt}$ female and *Pclo*$^{wt:wt}$ male rats
Video supplement 4. Atypical precopulatory behavior displayed between *Pclo*$^{wt:wt}$ female and *Pclo*$^{gt:gt}$ male rats
Video supplement 5. Atypical conspecific social interactions displayed between *Pclo*$^{gt:gt}$ and *Pclo*$^{wt:wt}$ male rats

n=8/genotype) (*Figure 6 - Supplement video 3 and 4*). Instinctive, pre-copulatory social interactions that normally occur between female and male rats, including courtship, grooming and genital investigation were effectively suppressed in female and male *Pclo*$^{gt/gt}$ rats (*Figure 6 – Supplement videos 3 and 4*).

In contrast to highly compatible precopulatory behavior shared between *Pclo*$^{wt/wt}$ and/or *Pclo*$^{gt/wt}$ rats, the social phenotype displayed by *Pclo*$^{gt/gt}$ rats of both sexes included overt aggression, biting, lunging and posturing (*Figure 6B; Figure 6 – Supplement videos 4 and 5*). By ~3 months of age, male *Pclo*$^{gt/gt}$ rats became socially incompatible and could not be housed with male or female littermates, independent of littermate genotype (n=14 *Pclo*$^{gt/gt}$ rats). Thus, *Pclo*-dependent neural connections in rats function to regulate conspecific chemosensory responses that mediate innate pre-copulatory social behavior required for progression to copulation (Sokolowski and Corbin, 2012) (*Figure 6C*).

Recessive *Pclo* traits are mappable to allelic markers for major depressive disorder

Mapping to a recessive phenotype, the *Synaptic Transmission* category also included a severely compromised *Glutamatergic Excitation* gene set (GO:0051966, p=0.00000001) in the brain of *Pclo*$^{gt/gt}$ rats (e.g. DEGs in the *Pclo*$^{gt/gt}$, but not in *Pclo*$^{gt/wt}$ mutants) (*Figure 5 – Source data 1*). *Pclo* clustered with *Grm5*, *Htr2a, Negr1, Drd2, Cacna2D1* and *Dlg1* (Dunn et al., 2014) as transcripts selectively down-regulated in *Pclo*$^{gt/gt}$ rats (Cluster 1, *Figure 7A*). Among the most significantly downregulated genes were *Grm5* (Glutamate Metabotropic Receptor 5) and *Htr2a* (the serotonin [5-Hydroxytryptamine] Receptor 2A) (*Figure 4 – Source data 1*). Both *Grm5* and *Htr2a* function as GPCRs in the signaling cascade that controls calcium mobilization and PKC activation (Dunn et al., 2014; Gereau and Heinemann, 1998). Alongside *glutamatergic* neurotransmission, *dopaminergic* neurotransmission (e.g. *Drd2*) and *Calcium signaling* (e.g. *Cacna2D1 and Dlg1*) also contributed to the recessive phenotype in *Pclo* mutants (*Figure 5 – Source data 1*).

Intriguingly, *Pclo*, *Grm5*, *Cacna2D1, Negr1, Sorcs3* and *Drd2* are among 44 genes recently reported to be key risk factors of major depressive disorder (MDD) (*Figure 7B*) identified by a human genome-wide association study containing 135,458 MDD cases and 334,901 controls (Wray et al., 2018).

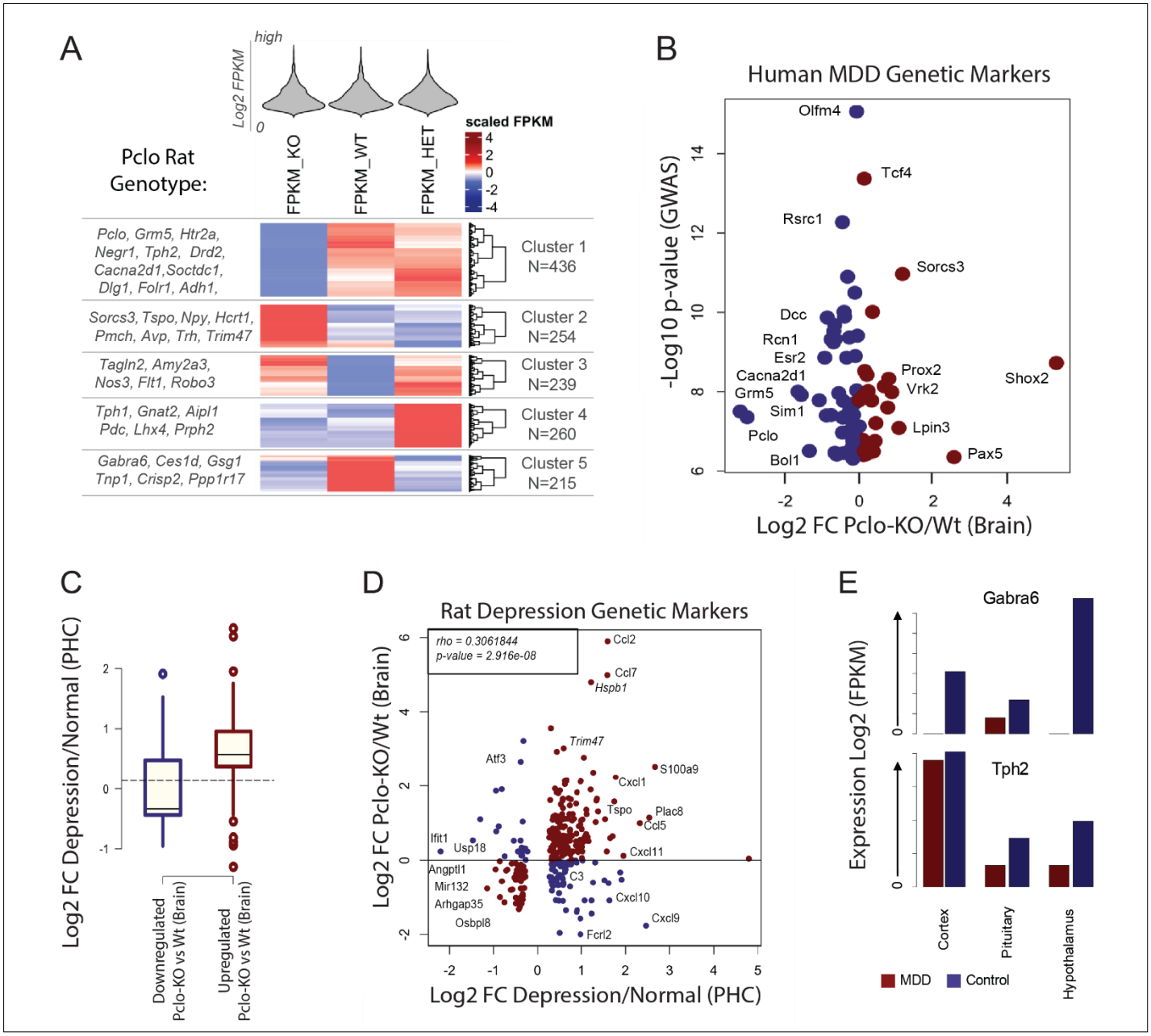

Figure 7. Piccolo deficiency RNA endophenotypes link to depression gene profiles

(**A**) Cluster Analysis of differentially expressed genes (DEGs) in *Pclo*$^{wt:wt}$ (WT), *Pclo*$^{wt:gt}$ (HET) and *Pclo*$^{gt:gt}$ (KO) rats.

(**B**) DEGs in *Pclo*$^{gt:gt}$ vs *Pclo*$^{wt:wt}$ (KO/Wt) rat brains are among major loci identified by human GWAS as MDD risk factors.

(**C**) Dysregulated genes in *Pclo*-KO versus Wt depressed rats. Note the significance level of correlated genes.

(**D**) Comparison between DEGs in depressed vs normal wt rat neruons and DEGs in *Pclo*-KO vs *Pclo*-Wt rat brains. Red dots are showing a similar pattern of expression (rho > 0.3).

(**E**) *Gabra6* as prominent gene dysregulated in *Pclo*-KO rat brains is not detected in Pituitary and Hypothalamus of depressed rats (*top*). Depression-related marker *Tph2* shown in comparison (*bottom*).

To test a potential relationship between Piccolo and depression, we data-mined and compared the transcriptome of an MDD rat model (Wang et al., 2017) to the transcriptome of our *Pclo*$^{gt/gt}$ rat brain (*Figure 7C*). Our strategy identified a robust list of 408 genes that were similarly affected in both models (*rho = 0.306* and *p-value = 2.916e-08*) (*Figure 7D*) supporting a transcriptome-level relationship between the biological processes dysregulated in *Pclo*$^{gt/gt}$ rats and neurological disorders categorized as MDD. Notably, the shared list of MDD transcripts encoded genes that have been associated with various features of depression, such as cortical dementia (e.g. *Trim47*), moodiness (e.g. *S100A9*), enhanced microglial activation (e.g. *Tspo*) and depression followed by immune challenge (e.g. *Figure 7D*). Interestingly, *Gabra6,* among the most highly dysregulated genes in *Pclo* KO rats, was also not detectable in the hypothalamus of depressed rats (*Figure 7E*), supporting the association of human *Pclo* and *Gabra6* variants with MDD (Inoue et al., 2015; Sullivan et al., 2009).

Cross-species analysis reveals robust differences in rat reproduction mutant phenotypes

We compared our phenotypes in rats to mutant phenotypes recorded in other species harboring loss-of-function mutations in orthologous genes (*Figure 2 – Source data 3*). Nine mutated rat genes (*Atg13*, *Btrc*, *Dlg1*, *Grik3*, *Pclo*, *Slc1a3, Spaca6, Zmynd8*, and *Ube2k*) have mutated orthologs in mice [(Mouse Genome Informatics (MGI), the International Mouse Phenotype Consortium (IMPC) and the National Center for Biological Information (NCBI) databases)], while 5 of our mutated orthologs have been characterized in plants, yeast, worms, flies or frogs (*Alk3, Atg13*, *Btrc*, *Dlg1*, *Pan3*) (*Figure 2 – Source data 3*).

In humans, genome-wide association studies (GWAS) have implicated orthologs for 12 of the mutant rat genes we analyzed (*Abca13*, *Alk3*, *Atg13*, *Btrc*, *Dlg1*, *Exoc6b*, *Fstl5*, *Gsgl1*, *Grik3, Pclo, Slc1a3*, *Ube2q2*) as either risk factors or candidate risk factors for various human disease processes (*Figure 2 – Source data 3*). About half of these later disease factors are associated with neurological/behavioral disorders (e. g. *Abca13*, *Dlg1*, *Exoc6b*, *Grik3, Pclo, Slc1a3*) (*Figure 2 – Source data 3*). Strikingly, the 'shortened life span' caused by mutations in *Atg13* has been reported across multiple species including plants, yeast, worms, flies, mice and rats (*Figure 2 – Source data 3*). In the hypomorphic *Atg13*$^{gt/gt}$ rats, a shortened life span was uniquely mapped to Atg13's carboxyl-terminal polypeptide (*Figure 3A-B*).

Interestingly, both *Pclo*$^{gt/gt}$ and *Dlg1*$^{gt/wt}$ rats displayed reduced fecundity and antisocial behavior (*Figure 2 – Source data 3*). *Dlg1* (a.k.a. *Synapse-Associated Protein 97* or *SAP97*) represented the most downregulated Calcium Signaling GO: gene in *Pclo*$^{gt/gt}$ rats (*Figure 5 – Figure supplement 2B*). Like our findings in *Pclo*$^{gt/gt}$ and *Dlg1*$^{gt/wt}$ rats, a *Dlg1*-null mutation was reported to disrupt courtship and mating in flies (Mendoza-Topaz et al., 2008)(*Figure 2 – Source data 3*). Thus, our mutant screen in rats unveiled a potential connection between *Pclo* and *Dlg1* to regulate conspecific social behavior.

Our comparative analysis also provided several examples where gene mutations analyzed here in rats produced significantly different phenotypes in another species with orthologous gene mutations (*Figure 2 – Source data 3*). Such differences may reflect the quality of the knockout and/or species-dependent differences in biology. As a prime example, while fertility and behavior is normal in *Pclo*-deficient mice (Mukherjee et al., 2010), our studies in rats revealed a genetic link between *Pclo*, sexual motivation, aggression and depression (*Figure 4B; Figure 7 – Videos 1-5*). Thus, *Pclo*$^{gt/gt}$ rats appear to better model *Pclo*-dependent limbic system effects on emotional processing in humans diagnosed with MDD (Woudstra et al., 2012; Woudstra et al., 2013). Curiously, while both *Piccolo* and *Gabra6* variants are associated with MDD and altered emotional processing based on studies in humans (Inoue et al., 2015; Sullivan et al., 2009), no direct sexual connection to either gene has been reported in humans. A most recent study, however, reports that the depression-associated *Pclo* rs2522833 C allele was less common in MDD patients presenting a family history of MDD (Zalar et al., 2018).

Discussion

Here, we identify a pool of 12 distinct mutant rat strains that are unable to reproduce (*Alk3, Atg13*, *Dlg1*, *Btrc*, *Exoc6b*, *Pan3*, *Pclo, Slc1a3*, *Spaca6*, *Tmx4*, *Ube2k*, *Zmynd8*). The mutant rat strain pool was derived from a library of recombinant spermatogonial stem cells harboring randomly inserted *Sleeping Beauty* genetrap transposons (Izsvak et al., 2010). The reproduction phenotypes we identified in rats were all associated with different steps in spermatogenesis or embryonic lethality except for three mutant strains (*Atg13*, *Dlg1*, *Pclo*). Of the later mutants, *Atg13* and *Pclo* strains stood out by exhibiting a "complex" phenotype that allowed us to decipher novel aspects of reproduction.

Our *Atg13*$^{gt/gt}$ rats displayed abnormal autophagy markers, gross renal abnormalities and inflammation-like phenotypes that preceded death in early adulthood. Atg13 (Autophagy related 13) is the master metabolic sensor for toggling between AMPK1-dependent cellular torpor (i.e. autophagy) and ULK1-repressed mTORC1-dependent cell growth. The *Atg13*$^{gt/gt}$ rat phenotype might be related to the loss of a phylogenetically conserved Ulk1-binding peptide encoded by *Atg13*'s terminal exon (*Figure 3A*). *Atg13*'s COOH-terminus has been implicated in activating the main autophagy-initiating complex (Hieke et al., 2015). Similar to the rat *Atg13*$^{gt/gt}$ phenotype, dysfunctions in *Atg13* have been associated with nephrological/immunological problems and autophagy in humans (Bronson et al., 2016; Ferreira et al., 2010). Mice harboring either a frameshift mutation in *Atg13* exon 5 or a genetrap in *Atg13* exon 1, by contrast, exhibit a more severe phenotype and die *in utero* due to heart defects (Kaizuka and Mizushima, 2016). Notably, the end-stage pathology of *Atg13*$^{gt/gt}$ rats correlated with immotile, degenerating caudal epididymal spermatozoa, likely associated with the premature aging phenotype.

While the *Atg13*$^{gt/gt}$ rat represents an excellent model to study the connection between premature aging, fitness and fertility, our *Pclo* mutant highlighted how traits linked to human neurological disorders can disrupt rat reproductive behavior. Curiously, the *Pclo*$^{SB\Delta 4\text{-}25}$ mutation disrupted reproduction, but induced more "global" changes in the brain transcriptome than in the testis, suggesting a possible crosstalk between the brain and gonads. The most significant changes in both tissues affected GABAergic signaling via GABA(A) receptors. Our data support a scenario, where the infertility phenotype is connected to the altered composition of GABA(A) receptor subunits associated with the GnRH signaling cascade.

Notably, GABA has been shown to play an important role in the maturation of gonadotrophin-releasing hormone (GnRH)-1 neurons during development and in regulating the pulsatile release of GnRH in adults (Herbison and Moenter, 2011; Temple and Wray, 2005; Watanabe et al., 2014). Altered neurological processes in *Pclo*$^{SB\Delta4\text{-}25}$ homozygotes appeared to affect the GnRH signaling cascade on multiple levels, including mis-regulation of *Heterotrimeric G-protein-coupled receptor* (GPCR) genes, *Ca^{2+} signaling* genes (*Figure 5 – Figure supplement 1A, 2A and 2B*) and up-regulated *neuropeptide* genes (Cluster 2, *Figure 7A*). Accordingly, impaired GnRH receptor signaling would translate into reduced responsiveness of testicular target genes (*Figure 5E-G*). Thus, our *Pclo*$^{SB\Delta4\text{-}25}$ mutant rat model holds potential to help address the long-standing debates on how GABAergic tone in the brain and testes is functionally linked to *GnRH neuron receptor activity* (Henderson, 2007) and reproductive behavior (Boehm et al., 2005; Yoon et al., 2005).

The *Pclo*$^{SB\Delta4\text{-}25}$ rat model exhibited additional GABAergic neuropathies. Both homo and heterozygous *Pclo*$^{SB\Delta4\text{-}25}$ rats develop generalized seizures (*Figure 6A*), similar to seizures observed in children homozygous for *Pclo*$^{\Delta6\text{-}stop}$ of *pontocerebellar hypoplasia type 3a* (Ahmed et al., 2015). Disturbed *GABAergic synaptic transmission* in *Pclo* mutants likely affects the balance between inhibition and excitation and thereby provokes seizures, manifesting itself as epileptiform activity (Herbison and Moenter, 2011; Watanabe et al., 2014). The functional significance of the tight control of *Gabra6* expression by *Pclo* has yet to be investigated, but one possibility is that a loss of synaptic integrity leads to its down-regulation (Waites et al., 2013). Even so, reports on *Gabra6* KO mice suggest that they exhibit no behavioral phenotypes (Homanics et al., 1997; Korpi et al., 1999), indicating that the complexity of phenotypes observed in *Pclo*$^{gt/gt}$ rats may not be entirely explained by *Gabra6*-deficiency alone. The most significantly dysregulated gene in Pclo$^{gt/gt}$ rat testes also encodes a GABA(A) receptor, *Gabrg3, gamma subunit 3* (*Figure 4G*), suggesting that a crosstalk between brain and testes may also involve a mechanism that regulates *Gabrg3*-dependent GABAergic tone.

Intriguingly, among the differentially expressed genes in *Pclo*$^{SB\Delta4\text{-}25}$ rats, we found a clear association with depressive phenotypes and the transcriptomes in brains of rats modeling MDD (*Figure 7C-E*). The top candidates of depression-related genes identified here as DEGs in *Pclo* rats$^{SB\Delta4\text{-}25}$ were involved in *glutamatergic* and *dopaminergic* neurotransmission and *neuronal*

calcium signaling pathways, and further matched key allelic neurological markers identified independently in large scale GWAS cohorts of humans diagnosed with MDD (e.g. *Pclo*, *Grm5*, *Htr2a, Sorcs3, Negr1, Drd2*; *Figure 7B*) (Howard et al., 2018; Wray et al., 2018). The affective disorder and limbic system neurotransmission phenotypes reported in MDD patients harboring *Pclo* variants were shown to disrupt emotional processing in response to conspecific facial cues (Woudstra et al., 2012; Woudstra et al., 2013). By analogy, the pre-copulatory mating behavior and aggression phenotypes reported here in $Pclo^{SB\Delta4\text{-}25}$ rats demonstrate Piccolo's control over sensory responses to social cues (*Figure 4B, Figure 6B and Figure 6 - Video supplements 1-5*).

In contrast to neurological phenotypes caused by *Pclo* variants in rats reported here, mice that lack the full calcium sensing coil-coil domain encoded by *Pclo* exon 14 ($Pclo^{\Delta14}$ mice) behave normal and are fertile (Giniatullina et al., 2015; Mukherjee et al., 2010). While we did not measure a significant difference in homozygous $Pclo^{SB\Delta4\text{-}25}$ rat body weights (*Figure 2 – Source data 2*), homozygous $Pclo^{\Delta14}$ mice displayed reduced body weights and enhanced postnatal mortality, consistent with a negative energy balance (Mukherjee et al., 2010). In $Pclo^{SB\Delta4\text{-}25}$ rats, like in *Dlg1*-deficient flies (Mendoza-Topaz et al., 2008), reproduction abnormalities were attributed to suppressed pre-copulatory and copulatory behavior, along with enhanced aggressive behavior in either sex of $Pclo^{gt/gt}$ rats (*Figure 6B and Figure 6 – Supplement videos 1-5*). When compared to *Pclo*-dependent sensory responses in humans (Woudstra et al., 2012; Woudstra et al., 2013), *Pclo*-dependent reproductive behavior displayed by $Pclo^{SB\Delta4\text{-}25}$ rats points to compromised synaptic transmission in the olfactory system, limbic system and/or hypothalamus as brain regions impacted by *Pclo* deficiency (*Figure 6C*). Piccolo regulates efficient recycling of synaptic vesicles, perhaps explaining why Pclo loss of function contributes to neurological disorders (Ackermann et al., 2019).

In summary, by combining forward genetics in rats with bioinformatics we identified *Pclo* as a candidate reproductive factor that controls behavioral responses to conspecific sensory input. Studies can now be aimed at defining PCLO-dependent neural circuits in the rat that control social behavior, and prospectively, how PCLO-dependent neuroendocrine signaling integrates social responses with metabolism. Phenotypical diversity transmitted by our spermatogonia-derived *Sleeping Beauty* gene-trap mutants underscores the robustness of our forward genetic approach using the rat model.

Materials and Methods

Mutant rat strains

Mutant rat strains harboring *Sleeping Beauty Β-Geo* genetrap transposons were originally transmitted to F1 progeny from a donor recombinant spermatogonial stem cell library (Izsvak et al., 2010). Recipient males were bred with wildtype females to produce a random panel of mutant rat strains enriched with genetraps within protein coding genes(Izsvak et al., 2010). Eighteen heterozygous F1 mutant rat strains (*Figure 1B and Figure 1 – Source data 1*) derived from an original pool of >150 *Sleeping Beauty Β-Geo* genetrap strains (Cryopreserved at: UTRR RRIDs) (Izsvak et al., 2010) were maintained as live colonies due to an expressed interest in and/or requests for respective strains by researchers representing a broad spectrum of biomedical fields (*Figure 2 – Source data 1*). Rat protocols were approved by the Institutional Animal Care and Use Committee (IACUC) at UT-Southwestern Medical Center in Dallas, as certified by the Association for Assessment and Accreditation of Laboratory Animal Care International (AAALAC).

Rat breeding for forward screen

The pool of 18 heterozygous F1 *Sleeping Beauty* genetrap mutant rat strains was evaluated for their ability to reproduce (*Figure 2 – Source data 1*). Based on a ~11 kb deletion from mouse chromosome 17 that contained *Spaca6* and *Has1*, and that blocked sperm-egg fusion in mice (Lorenzetti et al., 2014), the *Spaca6*$^{gt/gt}$ mutant rat strain was included in the current study as a control strain that provided a genetrap hypothesized to disrupt reproduction in rats. Additionally, *Rgs22* $^{gt/gt}$ mutant rats were included as a control strain hypothesized not to disrupt reproduction. The transposon insertion within intron 2 of *Rgs22* was not predicted to truncate the RGS22 open reading frame due to its intronic genetrap cassette being inserted in the 3' to 5' orientation. To our knowledge, neither *Spaca6*-specific mutations nor *Rgs22*-specific mutations had previously been reported to disrupt reproduction.

Founder-derived F1 mutant progeny were crossed with wildtype rats to produce F2 mutants. Males and females for 17 of 18 F2 heterozygous mutant strains successfully produced littles, of which, mean litter sizes produced by 15 of the F2 heterozygous mutant strains were comparable in size to wildtype Harlan, Sprague Dawley rat stocks (*Figure 2 – Source data 1*). Only *Dlg1*$^{wt/gt}$ females were identified as sub-fertile after pairing heterozygotes with wildtype rats of opposite

sex for >10 months. One *Dlg1*$^{wt/gt}$ female produced a single mutant female in one total litter (n=4 pups); however, the second generation *Dlg1*$^{wt/gt}$ female failed to reproduce and litters after subsequent pairings with fertile males for 12 months. Male and female (F3) heterozygous mutants from the other 17 strains were generated from separately outbred parents (Harlan, SD) and paired at 3-4 months of age to generate F4 homozygous mutants. Heterozygous mutant pairs that produced litters and displayed markedly reduced Mendelian rates towards generation of homozygous mutant progeny were classified as embryonic lethal (i.e. no homozygous mutant F4 progeny; n>50 total pups/strain except for *Alk3*$^{wt/gt}$ mutants, where n=35). Viable F4 homozygous mutants were paired with proven wildtype breeders (Harlan, SD) of opposite sex between 3-4 months of age to identify recessive mutations that transmitted significant changes in mean litter size. If F4 homozygotes failed to generate progeny by 3-4 months after pairing with a wildtype breeder, they were paired with a second wildtype proven breeder from Harlan, SD. Genes were classified as required for rat reproductive success under our standard housing conditions if homozygous mutations blocked multiple F4 progeny (n=2-4 homozygous mutant breeders/sex) from producing any offspring after pairing with 2 consecutive wildtype proven breeders of similar age over a span of >10 months. Adult lethal homozygous *Atg13* mutants demonstrated health decline between 3-4 months of age (i.e. shortly after setting up breeder pairs).

Genotyping mutant rat progeny

Endogenous gene-specific PCR primers near *Sleeping Beauty* integration sites were used in combination with transposon-specific primers to genotype progeny from familial generations F1 and F2 for newly generated mutant rat lines. Genomic sites of transposon integration were defined in F1 progeny by splinkerette PCR(Izsvak et al., 2010) and sequence analysis alignment on genome build RGSC v3.4 (Rn4). Genotyping results were verified by Southern blot hybridization assays of genomic DNA digested with XmnI and XbaI using a probe specific for the *EGFP* transgene and the *LacZ* portion of the *β-Geo* insert in the *Sleeping Beauty* transposon(Izsvak et al., 2010). Restriction analysis by Southern blot estimated ~7 transposon integrations/stem cell genome, which following random segregation and ploidy reduction during meiosis yielded ~3.5 transposon integrations/donor-derived spermatozoa, or founder-derived mutant F1 pup(Izsvak et al., 2010). Phenotypes in *Atg13*, *Btrc*, *Pclo*, *Pan3*, *Spaca6* and *Ube2k Sleeping Beauty* mutant rat strains were analyzed in F4 animals produced from F3 breeder pairs harboring only

their respective, *Sleeping Beauty* transposon integration (i.e. single copy gene-trap transposon F3 mutants).

Phenotype database and literature analysis

European Conditional Mouse Mutagenesis Programme (EUCOMM), Knockout Mouse Project (KOMP), Mouse Genome Informatics (MGI), International Mouse Phenotype Consortium (IMPC) and National Center for Biological Information (NCBI) databases provided records on mouse gene orthologs. NCBI PubMed, Gene and the Rat Genome Database (RGD) provided records on rat gene orthologs. Human phenotypes for mutant orthologs were searched in publicly available NCBI Genetics and Medicine databases, including: PubMed, Gene, Online Mendelian Inheritance in Man (OMIM), Database of Genotypes and Phenotypes (dbGaP); and the National Human Genome Research Institute's Catalog of Published Genome Wide Association Studies (NHGRI GWAS Catalog). NCBI PubMed and Gene were searched to identify phenotypes available for *Arabidopsis*, *Saccharomyces*, *Caenorhabditis*, *Drosophila*, *Danio* and *Xenopus* species. PhenomicDB database verified results from above database searches across all species. Literature comparisons for phenotypes caused by mutations in rat and mouse orthologs published independent of the current study are summarized in *Figure 2 – Source data 3*. Embryonic lethality or postnatal lethality prior to reproductive age was categorized as blocking reproduction. Fishers Exact t-test (two-tailed) was used to analyze phenotypic proportions of viable versus sub-viable, viable versus embryonic lethal, fertile versus infertile, mating versus non-mating.

Electroencephalogram (EEG) recording and analysis

Twelve adult rats (6 male, 6 female) were surgically prepared for EEG experiments with 4 rats in each experimental group (*Pclo*$^{wt/wt}$, *Pclo*$^{wt/gt}$, *Pclo*$^{gt/gt}$). Rats were anesthetized using a gas anesthesia machine with ~3% isoflurane in a 1 L/min mixture of 70% nitrous oxide and 30% oxygen. Four epidural recording electrodes made from #00-90 x 1/8 inch stainless steel screws were placed at the following stereotaxic coordinates: A-P ±2.0 mm, lateral ±3.0 mm and A-P - 4.0 mm, lateral ±3.0 mm along with a reference and ground screw over the olfactory bulb and cerebellum, respectively. Electrodes were attached by a flexible wire (kynar, 30 ga) to a custom 6-pin micro-connector (Omnetics) and secured with dental acrylic. Rats received the analgesic buprenorphine (0.05 mg/kg) as necessary following surgery and were allowed to recover for at

least 7 days prior to any experimentation. Following recovery from electrode implantation, each rat was placed in a custom acrylic recording cage (Marsh Designs, Peoria, AZ) and connected to a Tucker-Davis Technologies (Alachua, FL) RZ2/PZ3 neurophysiology workstation through a flexible cable suspended from the top of the cage with an interposed commutator to allow rats free access to food and water without twisting the cable. Continuous video/EEG (300 Hz sampling) was recorded for each rat simultaneously for 7 days and read by a user blinded to the experimental grouping for the presence of seizures and epileptiform activity. Seizure activity was marked at the beginning and end of each event to account for seizure duration, and the numbers of seizures per hour were calculated.

Western blot analysis

To analyze Piccolo expression, brains were dissected from wildtype, heterozygous mutant, and homozygous mutant Sprague Dawley rats and homogenized in 1.5 ml/0.5g tissue, ice-cold lysis buffer (50 mM HEPES, pH 8.0, 150 mM NaCl, 1 mM EDTA, 10% glycerol, 1% Triton X-100, 10 µg/ml aprotinin, 10 µg/ml leupeptin and 1 protease inhibitor tablet/12.5 ml) for 30s using a PTA-7 probe, setting 5, PT10-35 polytron (Kinematica). The homogenates were incubated on ice for 15–20 min and then centrifuged at 3000x*g* for 10 min at 4°C in a GPR tabletop centrifuge (Beckman, Inc.). The supernatant solutions were centrifuged at 15,800x*g* for 15 min at 4°C in a microcentrifuge (Model 5042, Eppendorf, Inc.) and the resultant supernatant fractions were stored at -80°C. 160 µg of protein was separated on 4-15% Mini-Protean TGX gels (BioRad, Inc.), and then transferred to nitrocellulose. Samples were not heated prior to loading. Nonspecific, protein binding sites were blocked by incubating membranes overnight at 4°C in blocking buffer: TBST (Tris-buffered saline with Tween-20: 10 mM Tris–HCl, pH 7.5, 150 mM NaCl, 0.1% Tween-20) containing 5% nonfat dry milk. Membranes were washed three times in TBST and incubated for 1 h at 22–24°C using rabbit anti-Piccolo (Synaptic Systems cat. no. 142002) diluted 1:2000 in blocking buffer. Membranes were washed three times in TBST (0.3% Tween-20) and incubated 45 min, 22-24°C with peroxidase-conjugated, anti-rabbit IgG (Jackson Immunoresearch) diluted 1:50,000 in blocking buffer. Membranes were washed three times in TBST and protein bands detected using the enhanced chemiluminescence detection method (ECL, Amersham, Inc.). Blots were stripped and re-probed with 1:20,000 dilution of mouse anti-TUBA1a (MU-121-UC, Biogenex, Inc.).

Rat embryonic fibroblast (REF) cultures were extracted in RIPA buffer (50 mM Tris pH 7.4, 150 mM sodium chloride, 1 mM EDTA, 1% IPEGAL, 0.25% deoxycholic acid) plus protease inhibitor and phosphatase inhibitor tablets (Roche Applied Science). 11 µg protein was separated on NuPAGE 4-12% Bis-Tris gels (Invitrogen, Inc.) and then transferred to nitrocellulose membranes. Nonspecific protein binding sites were blocked by incubating membranes overnight at 4°C in blocking buffer: TBS (Tris-buffered saline: 10 mM Tris–HCl, pH 7.4, 150 mM NaCl) containing 1X Western Blocking Reagent (Roche Applied Science, Inc.). Antibodies were diluted in TBS containing 0.5X Western Blocking Reagent + 0.1%Tween-20. Membranes were incubated in primary antibody for 1-2 hours at 22-24°C. Membranes were washed 4 x 5 min in TBST (0.1%-0.3% Tween-20), incubated in IRDye secondary antibody for 45-60 min, washed again 4 x 5 min, and scanned on an Odyssey Classic Quantitative Fluorescence Imaging System, Model 9120, Licor Biosciences, Inc. Images were analyzed with Odyssey software version 3.0.21. Primary antibodies: Rabbit anti-LC3A from Cell Signaling Technology, Inc, #4599, 1:300; Mouse anti-Atg13 from Medical and Biological Laboratories, Ltd, #M183-3, 1:1000; Guinea pig Anti-p62 from Medical and Biological Laboratories, Ltd, #PM066., 1:2000. Secondary antibodies were all from Licor Biosciences: Goat anti-rabbit IRDye 800CW #926-32211, 1:15000; Goat anti-mouse IRdye 680LT 1:20000; Donkey anti-guinea pig IRDye 800CW #926-32411, 1:15000.

Sperm counts and copulation

Epididymides were harvested from adult rats between 120-180 days of age and dissected free of surrounding fat and connective tissue for measuring weights, counting spermatozoa and histological analysis. To estimate spermatozoa numbers/rat, each epididymal caput and cauda were dissected apart from the corpus and separately placed into 3.8 cm^2 wells of a 12 well plate containing 1.5 ml DHF12 nutrient media [Dulbecco's Modified Eagles Medium:Ham's F12 (1:1); Sigma, D8437] 1x antibiotic antimycotic solution (Invitrogen, cat. no. 15240-062). Spermatozoa were released by thoroughly mincing each epididymal piece for 30 sec and allowing the spermatozoa to disperse into the medium for 25 min. Large pieces of epididymal tissue were removed with forceps and discarded. One ml of the epididymal cell-containing medium was carefully filtered through a 100 µm cell strainer (BD Biosciences, Inc.) into a 1.5 ml microfuge tube prior to counting using a Hemocytometer chamber. To assess breeding behavior and detect copulation, rats were paired with a single wildtype mate just prior to the end of the daily light cycle (4:00-5:00 pm central standard time). The following morning (7:00-8:00 am central

standard time), each female was examined for the presence of spermatozoa in the vagina. A foam swab tip was used to collect a vaginal smear, which was then analyzed by phase contrast microscopy to detect presence of sperm.

ELISA on Rat Plasma

Plasma LH and FSH levels were measured using ELISA Kits from CUSABIO according to the manufacturer's instructions (Rat FSH Cat# CSB-E06869R; Rat LH Cat# CSB-E12654r from CUSABIO).

Rat embryonic fibroblast culture

Primary rat embryonic fibroblast (REF) cultures were prepared from E14.5 embryos dissected from wildtype female rats after mating with *Atg13*$^{wt/gt}$ male rats. Timed mating was established as described above in the section on *Sperm Counts and Copulation*. Uteri were dissected from pregnant females and washed with 10 ml DHF12 medium, 1% Penicillin-Streptomycin solution (v/v). The heads and visceral tissue were removed from each isolated embryo. Visceral tissue was discarded. Tissue from the upper portion of the head was used to isolate genomic DNA and genotype embryos for the *Atg13* genetrap mutation. The remaining thoracic portion was washed in fresh DHF12 medium, transferred into tubes containing 5 ml 0.05% trypsin/1mM EDTA solution, minced for 2 minutes and then incubated at 37^{o}C for 20 min. After incubation, REF culture medium [DMEM (Sigma, D5648-10XL), 10% fetal bovine serum (Tissue Culture Biologicals, 104300), 1% Penicillin/Streptomycin (Hyclone, SV30010)] was added to the cell suspension and the cells were dissociated further by gentle trituration (5 strokes) using a p1000 Eppendorf tip. The cell suspension was centrifuged 4 min at 120 x *g* and the supernatant was discarded. The cellular pellet was retained, suspended to 15 ml in fresh REF medium, plated into 10cm plastic tissue culture dishes (Corning, Inc.) and then incubated at 37^{o}C, 5% CO_2 overnight. REFs were fed 15 ml fresh medium every 48 hrs, and sub-cultured using the 0.05% trypsin/1mM EDTA solution to harvest attached cells from culture dishes every 2-3 days. Harvested REFs were passaged by plating at ~10^4 cells/cm^2 in 3 ml/cm^2 REF medium. REF cultures were maintained at 37^{o}C, 5% CO_2, and used for experiments at passage 4. REFs were treated for 24 hr with or without 3 mM ammonium chloride (Fluka, 09718), 100 nM Rapamycin A (LC Laboratories, R-5000) and, or 3 nM Bafilomycin A1 (Sigma, B1793) prior to preparing lysates for western blots.

Histological sectioning and staining

Hematoxylin/Eosin (H&E), periodic acid-Schiff's (PAS) and Trichrome staining on histological sections from rat tissues were conducted by standard procedures at the Molecular Pathology Core Laboratory, UT Southwestern Medical Center in Dallas.

Preparing frozen sections

To prepare frozen testis sections for labeling with antibodies, testes were dissected from rats, perforated by puncturing three equally spaced holes in the *tunica albuginea* along each longitudinal axis of the testis using a 27 gauge needle, and fixed for ~18 hr at 4°C in 0.1M sodium phosphate buffer, pH 7.2, containing 4% paraformaldehyde. Fixed testes were equilibrated through a 10%, 18% and 25% sucrose [wt/v, dissolved in 1x phosphate buffered saline (PBS; Invitrogen Inc, cat no. 14040-182)] gradient by sequential overnight incubations (~24 hr) at 4°C in 20 ml of each respective sucrose solution. Once equilibrated to 25% sucrose, testes were embedded in tissue freezing medium (Electron Microscopy Sciences Inc., #72592) and frozen using a Shandon Lipshaw (#45972) cryo-bath. Frozen testes were used to prepare a parallel series of 8 µm cryo-sections. Frozen sections were stored at -40°C until use in immunofluorescence assays as described below.

Fluorescence immunohistochemistry

Prior to labeling studies, sections were equilibrated in air to ~22-24ºC for 15 min, hydrated in Dulbecco's phosphate-buffered saline (PBS) (Sigma, D8537) at 22-24ºC for 10 min, heat-treated at 80°C for 8 minutes in 10 mM sodium citrate (pH 6.0) and then incubated for 1 hr at 22-24ºC in blocking buffer [Roche Blocking Reagent (1% v/v) diluted in 0.1M Sodium phosphate buffer, containing Triton X100 (0.1% v/v)]. Sections were then treated for 18-24 hr at 22-24ºC with respective antibodies diluted in blocking buffer at the following concentrations: [1:400 mouse anti-Sall4 IgG (H00057167-M03, Abnova, Inc); 1:400 rabbit anti-phospho-H2A.X (Ser139) IgG (07-164, Millipore, Inc); 1:400 rabbit anti-phospho-Histone H3 (ser10) IgG (06-570, Millipore, Inc)] diluted into Roche blocking (1% w/v) reagent. After treatment with primary antibodies, sections were washed 3 times for 10 min/wash in 50 ml PBS and then incubated for 40 min at 22-24ºC with respective AlexaFluor594 (Invitrogen, Inc), or AlexaFluor488 (Invitrogen, Inc) secondary antibodies diluted to 4 µg/ml in PBS containing 5 µg/ml Hoechst 33342 dye (Molecular probes, cat no. H3570). After treatment with secondary antibodies, sections were washed 3 times at 10

min/wash in 50 ml PBS. After the 3rd wash in PBS, sections were cover-slipped for viewing using Fluorogel mounting medium (Electron Microscopy sciences, cat no. 17985-10). Images were acquired using an IX70 Olympus fluorescence microscope (Olympus Inc.) equipped with Simple-PCI imaging software (C-Imaging Systems, Compix, Cranberry Township, PA).

Perfusion, Sectioning and Immunohistochemistry of rat brains

Perfusion: Adult rats (P100) were first sedated in Isoflurane (Abbott GmbH & Co. KG, Wiesbaden, Germany) and then deeply anesthetized with a mix of 20 mg/ml Xylavet (CO-pharma, Burgdorf, Germany), 100 mg/ml Ketamin (Inresa Arzneimittel GmbH, Freiburg, Germany) in 0.9% NaCl (B/BRAUN, Melsungen, Germany). Afterwards the heart was made accessible by opening the thoracic cavity, and a needle inserted into the left ventricle and the atrium cut open with a small scissor. Animals were initially perfused with PBS and then with freshly made 4 % PFA, before dissecting and further incubated for 24h in 4 % PFA at 4°C. Brains were then cryoprotected in 15% and then 30% sucrose at 4°C for 24h. Brains were then frozen using 2-methylbutane (#3927.1, Carl-Roth, Karlsruhe, Germany) cooled with dry ice to -50°C and stored at -20°C.

Brain sectioning. 20 µm thin serial sections were cut from frozen brains using a cryostat (Leica Mikrosysteme Vertrieb GmbH, Wetzlar, Germany). Slices transferred to a microscope slide (Superfrost Plus, #H867.1, Gerhard Menzel B.V. & Co. KG, Braunschweig, Germany), dried at RT for at least 1h and stored at -20°C.

Immunohistochemistry. 3,3'-Diaminobenzidine (DAB) staining of 20 µm coronal brain sections labeled with mouse anti GnRH antibody performed as previous described (Brinschwitz et al., 2010). In brief, thawed sections were dried for 30 min at RT and washed 3x for 10 min in PBS-T (PBS 1X (Thermo Fisher Scientific, Waltham, USA) + 0.025% Triton X-100 (#3051.2, Carl-Roth, Karlsruhe, Germany) and endogenous peroxidase was blocked for 10 min with 0.3% H2O2 in PBS, before blocking for 2h at RT in blocking solution (PBS plus 10% normal goat serum and 1% BSA). Sections were then incubated in primary mouse anti GnRH antibody (1:500, HU4H, provided by H. Urbanski, Oregon Regional Primary Center, Beaverton, OR) in blocking solution for 1h at RT and 2 days at 4°C. After washing sections were incubated in a secondary Biotin-conjugated antibody (goat anti mouse Biotin-SP, 1:1000, #115-035-003, Dianova GmbH, Hamburg, Germany) in blocking solution for 1h at RT and 2 days at 4°C, before adding the ABC reaction reagent

(Vectastain ABC Kit #PK-6100, Vector Laboratories Inc., Burlingame, CA) for 1h at RT and 1 day at 4°C. After 1 day, sections were washed before adding the DAB solution (DAB peroxidase substrate Kit #SK-4100, Vector Laboratories Inc., Burlingame, CA) for 1min. DAB reaction was stopped with purified water (ddH2O) and sections were dehydrated in the following sequence: 2 min 70 % ethanol (EtOH), 2 min 80 % EtOH, 2 min 95 % EtOH, 2 min 99,9% EtOH. Sections were cleared in Rotihistol (#6640.4, Carl Roth GmbH, Karlsruhe, Germany) until mounting in Entellan (#1.07961.0100, Merck KGaA, Darmstadt, Germany).

Analysis of RNA-seq data from Pclo rats

Single end 100 bp RNA-seq libraries were prepared from brain, liver and testis tissues of ~6-month-old $Pclo^{gt/gt}$, $Pclo^{gt/wt}$, $Pclo^{wt/wt}$ rats. The libraries were run on *Illumina Hiseq 2000* sequencer (Total number of reads was ~550-600 million). For *basecalling* we used the *Illumina Casava1.7* software. Reads were than aligned to the reference human genome version *rn6* by using *Tophat2/bowtie2*. This approach has provided a *refseq_rn6* gene model that guided the assembly process of the transcriptome. We checked the quality of the sequencing and the mapping by *Fastqc* and by *RNASeqQC*, repectively. Due to the negligible technical variances, the read counts of a gene had a Poisson distribution, thus we could apply the single-replicate model to analyze the data. We calculated Read counts using *featureCounts* from the *subread package (http://subread.sourceforge.net/).* Fragments Per Kiolobase of RNA per Million mapped reads (FPKM) was calculated using *bamutils (http://ngsutils.org/modules/bamutils/count/).*

Analysis of differentially expressed genes

Random Variable1 (*Var1*) = *n.l.x*, where *x* (Random Variable2) is the expression level of a gene (e.g., in RPKM (Reads Per Kilo bases per Million reads) *n* is reflecting the sequencing depth and *l* is the gene length. The method proposed by Anders and Huber was used to calculate *n*(Anders and Huber, 2010). To generate more robust and accurate *Fold change* values from unreplicated RNA-seq data, we determined the normalization constant and variance by pasting the two random variables in the published algorithm of: (http://bioinformatics.oxfordjournals.org/content/early/2012/08/23/bioinformatics.bts515.full.pdf+html). To identify the Gene Ontology (GO) categories that were overrepresented in the Piccolo mutants, we compared samples from the brain and testis of $Pclo^{gt/gt}$ and $Pclo^{wt/gt}$ vs $Pclo^{wt/wt}$ rats, with the entire set of rat genes as a background.

Acknowledgments

This work was supported by National Institutes of Health grants to F.K.H. from The Eunice Kennedy Shriver National Institute of Child Health and Human Development: R01HD053889 and R01HD061575, The National Center for Research Resources: R24RR03232601; and The Office of the Director: R24OD011108. Neurological analyses on *Pclo* mutant rats were conducted by The Neuro-Models Facility (EJP, LBG) at UT Southwestern Medical Center, and supported by the Haggerty Center for Brain Injury and Repair. Z. Iv. was supported by grants from the Bundesministerium für Bildung und Forschung (NGFN-2, NGFNplus - ENGINE). Z. Iz. is supported by European Research Council, ERC Advanced [ERC-2011-AdG 294742]. CG is supported by the German Center for Neurodegenerative Diseases (DZNE) and DFG-SFB958. We thank Christine Römer and Ruth Ann Word for their critical comments.

REFERENCES

Ackermann, F., Schink, K.O., Bruns, C., Izsvák, Z., Hamra, F.K., Rosenmund, C., and Garner, A.M. (2019). Critical role for piccolo in synaptic vesicle retrieval. eLife *8:e46629* DOI: 10.7554/eLife.46629.

Ahmed, M.Y., Chioza, B.A., Rajab, A., Schmitz-Abe, K., Al-Khayat, A., Al-Turki, S., Baple, E.L., Patton, M.A., Al-Memar, A.Y., Hurles, M.E., *et al.* (2015). Loss of PCLO function underlies pontocerebellar hypoplasia type III. Neurology *84*, 1745-1750.

Alers, S., Wesselborg, S., and Stork, B. (2014). ATG13: Just a companion, or an executor of the autophagic program? Autophagy *10*, 944-956.

Anders, S., and Huber, W. (2010). Differential expression analysis for sequence count data. Genome Biol *11*, R106.

Ayadi, A., Birling, M.C., Bottomley, J., Bussell, J., Fuchs, H., Fray, M., Gailus-Durner, V., Greenaway, S., Houghton, R., Karp, N., *et al.* (2012). Mouse large-scale phenotyping initiatives: overview of the European Mouse Disease Clinic (EUMODIC) and of the Wellcome Trust Sanger Institute Mouse Genetics Project. Mamm Genome *23*, 600-610.

Berridge, K.C., and Kringelbach, M.L. (2015). Pleasure systems in the brain. Neuron *86*, 646-664.

Boehm, U., Zou, Z., and Buck, L.B. (2005). Feedback loops link odor and pheromone signaling with reproduction. Cell *123*, 683-695.

Bosch, O.J. (2013). Maternal aggression in rodents: brain oxytocin and vasopressin mediate pup defence. Philos Trans R Soc Lond B Biol Sci *368*, 20130085.

Bronson, P.G., Chang, D., Bhangale, T., Seldin, M.F., Ortmann, W., Ferreira, R.C., Urcelay, E., Pereira, L.F., Martin, J., Plebani, A., *et al.* (2016). Common variants at PVT1, ATG13-AMBRA1, AHI1 and CLEC16A are associated with selective IgA deficiency. Nat Genet *48*, 1425-1429.

Carmel, P.W., Araki, S., and Ferin, M. (1976). Pituitary stalk portal blood collection in rhesus monkeys: evidence for pulsatile release of gonadotropin-releasing hormone (GnRH). Endocrinology *99*, 243-248.

Cases-Langhoff, C., Voss, B., Garner, A.M., Appeltauer, U., Takei, K., Kindler, S., Veh, R.W., De Camilli, P., Gundelfinger, E.D., and Garner, C.C. (1996). Piccolo, a novel 420 kDa protein associated with the presynaptic cytomatrix. Eur J Cell Biol *69*, 214-223.

Chen, P., and Hong, W. (2018). Neural Circuit Mechanisms of Social Behavior. Neuron *98*, 16-30.

Choi, K.H., Higgs, B.W., Wendland, J.R., Song, J., McMahon, F.J., and Webster, M.J. (2011). Gene expression and genetic variation data implicate PCLO in bipolar disorder. Biol Psychiatry *69*, 353-359.

Coria-Avila, G.A., Manzo, J., Garcia, L.I., Carrillo, P., Miquel, M., and Pfaus, J.G. (2014). Neurobiology of social attachments. Neurosci Biobehav Rev *43*, 173-182.

Dunn, H.A., Walther, C., Yuan, G.Y., Caetano, F.A., Godin, C.M., and Ferguson, S.S. (2014). Role of SAP97 in the regulation of 5-HT2AR endocytosis and signaling. Mol Pharmacol *86*, 275-283.

Ferreira, R.C., Pan-Hammarstrom, Q., Graham, R.R., Gateva, V., Fontan, G., Lee, A.T., Ortmann, W., Urcelay, E., Fernandez-Arquero, M., Nunez, C., *et al.* (2010). Association of IFIH1 and other autoimmunity risk alleles with selective IgA deficiency. Nat Genet *42*, 777-780.

Funakoshi, T., Matsuura, A., Noda, T., and Ohsumi, Y. (1997). Analyses of APG13 gene involved in autophagy in yeast, Saccharomyces cerevisiae. Gene *192*, 207-213.

Gereau, R.W.t., and Heinemann, S.F. (1998). Role of protein kinase C phosphorylation in rapid desensitization of metabotropic glutamate receptor 5. Neuron *20*, 143-151.

Gibbs, R.A., Weinstock, G.M., Metzker, M.L., Muzny, D.M., Sodergren, E.J., Scherer, S., Scott, G., Steffen, D., Worley, K.C., Burch, P.E., *et al.* (2004). Genome sequence of the Brown Norway rat yields insights into mammalian evolution. Nature *428*, 493-521.

Giniatullina, A., Maroteaux, G., Geerts, C.J., Koopmans, B., Loos, M., Klaassen, R., Chen, N., van der Schors, R.C., van Nierop, P., Li, K.W., *et al.* (2015). Functional characterization of the PCLO

p.Ser4814Ala variant associated with major depressive disorder reveals cellular but not behavioral differences. Neuroscience *300*, 518-538.

Giordano, M., Guemes, M., Lopez-Arias, V., and Paredes, R.G. (1998). Socio-sexual behavior in male rats after lesions of the dorsolateral tegmentum. Physiol Behav *65*, 89-94.

Henderson, L.P. (2007). Steroid modulation of GABAA receptor-mediated transmission in the hypothalamus: effects on reproductive function. Neuropharmacology *52*, 1439-1453.

Herbison, A.E., and Moenter, S.M. (2011). Depolarising and hyperpolarising actions of GABA(A) receptor activation on gonadotrophin-releasing hormone neurones: towards an emerging consensus. J Neuroendocrinol *23*, 557-569.

Hieke, N., Loffler, A.S., Kaizuka, T., Berleth, N., Bohler, P., Driessen, S., Stuhldreier, F., Friesen, O., Assani, K., Schmitz, K., *et al.* (2015). Expression of a ULK1/2 binding-deficient ATG13 variant can partially restore autophagic activity in ATG13-deficient cells. Autophagy *11*, 1471-1483.

Homanics, G.E., Ferguson, C., Quinlan, J.J., Daggett, J., Snyder, K., Lagenaur, C., Mi, Z.P., Wang, X.H., Grayson, D.R., and Firestone, L.L. (1997). Gene knockout of the alpha6 subunit of the gamma-aminobutyric acid type A receptor: lack of effect on responses to ethanol, pentobarbital, and general anesthetics. Mol Pharmacol *51*, 588-596.

Howard, D.M., Adams, M.J., Shirali, M., Clarke, T.K., Marioni, R.E., Davies, G., Coleman, J.R.I., Alloza, C., Shen, X., Barbu, M.C., *et al.* (2018). Genome-wide association study of depression phenotypes in UK Biobank identifies variants in excitatory synaptic pathways. Nat Commun *9*, 1470.

Inoue, A., Akiyoshi, J., Muronaga, M., Masuda, K., Aizawa, S., Hirakawa, H., Ishitobi, Y., Higuma, H., Maruyama, Y., Ninomiya, T., *et al.* (2015). Association of TMEM132D, COMT, and GABRA6 genotypes with cingulate, frontal cortex and hippocampal emotional processing in panic and major depressive disorder. Int J Psychiatry Clin Pract *19*, 192-200.

Ivics, Z., Hackett, P.B., Plasterk, R.H., and Izsvak, Z. (1997). Molecular reconstruction of Sleeping Beauty, a Tc1-like transposon from fish, and its transposition in human cells. Cell *91*, 501-510.

Izsvak, Z., Frohlich, J., Grabundzija, I., Shirley, J.R., Powell, H.M., Chapman, K.M., Ivics, Z., and Hamra, F.K. (2010). Generating knockout rats by transposon mutagenesis in spermatogonial stem cells. Nat Methods *7*, 443-445.

Izsvak, Z., Ivics, Z., and Plasterk, R.H. (2000). Sleeping Beauty, a wide host-range transposon vector for genetic transformation in vertebrates. J Mol Biol *302*, 93-102.

Kaizuka, T., and Mizushima, N. (2016). Atg13 is essential for autophagy and cardiac development in mice. Molecular and Cellular Biology *36*, 585-595.

Korpi, E.R., Koikkalainen, P., Vekovischeva, O.Y., Makela, R., Kleinz, R., Uusi-Oukari, M., and Wisden, W. (1999). Cerebellar granule-cell-specific GABAA receptors attenuate benzodiazepine-induced ataxia: evidence from alpha 6-subunit-deficient mice. Eur J Neurosci *11*, 233-240.

Lian, J., Watts, R., Quiroga, A.D., Beggs, M.R., Alexander, R.T., and Lehner, R. (2019). Ces1d deficiency protects against high-sucrose diet-induced hepatic triacylglycerol accumulation. J Lipid Res *60*, 880-891.

Lorenzetti, D., Poirier, C., Zhao, M., Overbeek, P.A., Harrison, W., and Bishop, C.E. (2014). A transgenic insertion on mouse chromosome 17 inactivates a novel immunoglobulin superfamily gene potentially involved in sperm-egg fusion. Mamm Genome *25*, 141-148.

Luquet, S., and Magnan, C. (2009). The central nervous system at the core of the regulation of energy homeostasis. Front Biosci (Schol Ed) *1*, 448-465.

Maclean, P.D. (1952). Some psychiatric implications of physiological studies on frontotemporal portion of limbic system (visceral brain). Electroencephalogr Clin Neurophysiol *4*, 407-418.

Matzuk, M.M., and Lamb, D.J. (2008). The biology of infertility: research advances and clinical challenges. Nat Med *14*, 1197-1213.

Mendoza-Topaz, C., Urra, F., Barria, R., Albornoz, V., Ugalde, D., Thomas, U., Gundelfinger, E.D., Delgado, R., Kukuljan, M., Sanxaridis, P.D., *et al.* (2008). DLGS97/SAP97 is developmentally

upregulated and is required for complex adult behaviors and synapse morphology and function. J Neurosci *28*, 304-314.

Mukherjee, K., Yang, X., Gerber, S.H., Kwon, H.B., Ho, A., Castillo, P.E., Liu, X., and Sudhof, T.C. (2010). Piccolo and bassoon maintain synaptic vesicle clustering without directly participating in vesicle exocytosis. Proc Natl Acad Sci U S A *107*, 6504-6509.

Petrulis, A. (2013a). Chemosignals and hormones in the neural control of mammalian sexual behavior. Front Neuroendocrinol *34*, 255-267.

Petrulis, A. (2013b). Chemosignals, hormones and mammalian reproduction. Horm Behav *63*, 723-741.

Phelps, E.A., and LeDoux, J.E. (2005). Contributions of the amygdala to emotion processing: from animal models to human behavior. Neuron *48*, 175-187.

Piet, R., Fraissenon, A., Boehm, U., and Herbison, A.E. (2015). Estrogen permits vasopressin signaling in preoptic kisspeptin neurons in the female mouse. J Neurosci *35*, 6881-6892.

Rupprecht, R., Papadopoulos, V., Rammes, G., Baghai, T.C., Fan, J., Akula, N., Groyer, G., Adams, D., and Schumacher, M. (2010). Translocator protein (18 kDa) (TSPO) as a therapeutic target for neurological and psychiatric disorders. Nat Rev Drug Discov *9*, 971-988.

Santoru, F., Berretti, R., Locci, A., Porcu, P., and Concas, A. (2014). Decreased allopregnanolone induced by hormonal contraceptives is associated with a reduction in social behavior and sexual motivation in female rats. Psychopharmacology (Berl) *231*, 3351-3364.

Sokolowski, K., and Corbin, J.G. (2012). Wired for behaviors: from development to function of innate limbic system circuitry. Front Mol Neurosci *5*, 55.

Spiegelstein, O., Cabrera, R.M., Bozinov, D., Wlodarczyk, B., and Finnell, R.H. (2004). Folate-regulated changes in gene expression in the anterior neural tube of folate binding protein-1 (Folbp1)-deficient murine embryos. Neurochem Res *29*, 1105-1112.

Sullivan, P.F., de Geus, E.J., Willemsen, G., James, M.R., Smit, J.H., Zandbelt, T., Arolt, V., Baune, B.T., Blackwood, D., Cichon, S., *et al.* (2009). Genome-wide association for major depressive disorder: a possible role for the presynaptic protein piccolo. Mol Psychiatry *14*, 359-375.

Suttangkakul, A., Li, F., Chung, T., and Vierstra, R.D. (2011). The ATG1/ATG13 protein kinase complex is both a regulator and a target of autophagic recycling in Arabidopsis. Plant Cell *23*, 3761-3779.

Temple, J.L., and Wray, S. (2005). Developmental changes in GABA receptor subunit composition within the gonadotrophin-releasing hormone-1 neuronal system. J Neuroendocrinol *17*, 591-599.

True, C., Grove, K.L., and Smith, M.S. (2011). Beyond Leptin: Emerging Candidates for the Integration of Metabolic and Reproductive Function during Negative Energy Balance. Front Endocrinol (Lausanne) *2*, 53.

Waites, C.L., Leal-Ortiz, S.A., Okerlund, N., Dalke, H., Fejtova, A., Altrock, W.D., Gundelfinger, E.D., and Garner, C.C. (2013). Bassoon and Piccolo maintain synapse integrity by regulating protein ubiquitination and degradation. EMBO J *32*, 954-969.

Wang, Y., Jiang, H., Meng, H., Lu, J., Li, J., Zhang, X., Yang, X., Zhao, B., Sun, Y., and Bao, T. (2017). Genome-wide transcriptome analysis of hippocampus in rats indicated that TLR/NLR signaling pathway was involved in the pathogenisis of depressive disorder induced by chronic restraint stress. Brain Res Bull *134*, 195-204.

Watanabe, M., Fukuda, A., and Nabekura, J. (2014). The role of GABA in the regulation of GnRH neurons. Front Neurosci *8*, 387.

Woudstra, S., Bochdanovits, Z., van Tol, M.J., Veltman, D.J., Zitman, F.G., van Buchem, M.A., van der Wee, N.J., Opmeer, E.M., Demenescu, L.R., Aleman, A., *et al.* (2012). Piccolo genotype modulates neural correlates of emotion processing but not executive functioning. Transl Psychiatry *2*, e99.

Woudstra, S., van Tol, M.J., Bochdanovits, Z., van der Wee, N.J., Zitman, F.G., van Buchem, M.A., Opmeer, E.M., Aleman, A., Penninx, B.W., Veltman, D.J., *et al.* (2013). Modulatory effects of the piccolo genotype on emotional memory in health and depression. PLoS One *8*, e61494.

949 Wray, N.R., Ripke, S., Mattheisen, M., Trzaskowski, M., Byrne, E.M., Abdellaoui, A., Adams, M.J.,
950 Agerbo, E., Air, T.M., Andlauer, T.M.F., *et al.* (2018). Genome-wide association analyses identify 44
951 risk variants and refine the genetic architecture of major depression. Nat Genet *50*, 668-681.
952 Yang, Y., Luo, J., Yu, D., Zhang, T., Lin, Q., Li, Q., Wu, X., Su, Z., Zhang, Q., Xiang, Q., *et al.* (2018).
953 Vitamin A Promotes Leydig Cell Differentiation via Alcohol Dehydrogenase 1. Front Endocrinol
954 (Lausanne) *9*, 644.
955 Yoon, H., Enquist, L.W., and Dulac, C. (2005). Olfactory inputs to hypothalamic neurons controlling
956 reproduction and fertility. Cell *123*, 669-682.
957 Zalar, B., Blatnik, A., Maver, A., Klemenc-Ketis, Z., and Peterlin, B. (2018). Family History as an
958 Important Factor for Stratifying Participants in Genetic Studies of Major Depression. Balkan J Med
959 Genet *21*, 5-12.
960 Zhou, W., Bolden-Tiller, O.U., Shetty, G., Shao, S.H., Weng, C.C., Pakarinen, P., Liu, Z., Stivers, D.N.,
961 and Meistrich, M.L. (2010). Changes in gene expression in somatic cells of rat testes resulting from
962 hormonal modulation and radiation-induced germ cell depletion. Biol Reprod *82*, 54-65.
963